SCIENCE CHINA
Earth Sciences

Dynamics of local extreme rainfall of super Typhoon Soudelor (2015) in East China

PAN Jinsong, TENG Daigao, ZHANG Fuqing, ZHOU Lingli, LUO Ling, WENG Yonghui and ZHANG Yunji

Citation: SCIENCE CHINA Earth Sciences ; doi: 10.1007/s11430-017-9135-6

View online: http://engine.scichina.com/doi/10.1007/s11430-017-9135-6

Published by the Science China Press

SCIENCE CHINA
Earth Sciences

•RESEARCH PAPER•

https://doi.org/10.1007/s11430-017-9135-6

Dynamics of local extreme rainfall of super Typhoon Soudelor (2015) in East China

Jinsong PAN[1,2], Daigao TENG[1,2*], Fuqing ZHANG[2], Lingli ZHOU[1], Ling LUO[1], Yonghui WENG[2] & Yunji ZHANG[2]

[1] *Zhejiang Meteorological Observatory, Hangzhou 310021, China;*
[2] *Department of Meteorology and Atmospheric Sciences, and Center for Advanced Data Assimilation and Prediction Techniques, Pennsylvania State University, University Park, Pennsylvania 16802, USA*

Received January 11, 2017; revised August 9, 2017; accepted November 3, 2017; published online February 3, 2018

Abstract The characteristics and dynamics associated with the distribution, intensity, and triggering factors of local severe precipitation in Zhejiang Province induced by Super Typhoon Soudelor (2015) were investigated using mesoscale surface observations, radar reflectivity, satellite nephograms, and the final (FNL) analyses of the Global Forecasting System (GFS) of the National Center for Environmental Prediction (NCEP). The rainfall processes during Soudelor's landfall and translation over East China could be separated into four stages based on rainfall characteristics such as distribution, intensity, and corresponding dynamics. The relatively less precipitation in the first stage resulted from interaction between the easterly wind to the north flank of this tropical cyclone (TC) and the coastal topography along the southeast of Zhejiang Province, China. With landfall of the TC in East China during the second stage, precipitation maxima occurred because of interaction between the TC's principal rainbands and the local topography from northeastern Fujian Province to southwestern Zhejiang Province. The distribution of precipitation presented significant asymmetric features in the third stage with maximal rainfall bands in the northeast quadrant of the TC when Soudelor's track turned from westward to northward as the TC decayed rapidly. Finally, during the northward to northeastward translation of the TC in the fourth stage, the interaction between a mid-latitude weather system and the northern part of the TC resulted in transfer of the maximum rainfall from the north of Zhejiang Province to the north of Jiangsu Province, which represented the end of rainfall in Zhejiang Province. Further quantitative calculations of the rainfall rate induced by the interaction between local topography and TC circulation (defined as "orographic effects") in the context of a one-dimensional simplified model showed that orographic effects were the primary factor determining the intensity of precipitation in this case, and accounted for over 50% of the total precipitation. The asymmetric distribution of the TC's rainbands was closely related to the asymmetric distribution of moisture resulted from changes of the TC's structure, and led to asymmetric distribution of local intense precipitation induced by Soudelor. Based on analysis of this TC, it could be concluded that local severe rainfall in the coastal regions of East China is closely related to changes of TC structure and intensity, as well as the outer rainbands. In addition, precipitation intensity and duration will increase correspondingly because of the complex interactions between the TC and local topography, and the particular TC track along large-scale steering flow. The results of this study may be useful for the understanding, prediction, and warning of disasters induced by local extreme rainfall caused by TCs, especially for facilitating forecasting and warning of flooding and mudslides associated with torrential rain caused by interactions between landfalling TCs and coastal topography.

Keywords TC outer circulation, TC principal rainband, Orographic effect, Expanding of TC's spiral bands

Citation: Pan J S, Teng D G, Zhang F Q, Zhou L L, Luo L, Weng Y H, Zhang Y J. 2018. Dynamics of local extreme rainfall of super Typhoon Soudelor (2015) in East China. Science China Earth Sciences, 61, https://doi.org/10.1007/s11430-017-9135-6

* Corresponding author (email: 520tdg@163.com)

1. Introduction

China is among the countries most impacted by landfalling tropical cyclones (LTCs) and suffers some of the most severe LTC disasters in the world (Chen and Meng, 2001). Hazards induced by tropical cyclones (TCs) include strong winds and storm surges (Emanuel, 2005; NHC, 2009). Many studies have verified and pre-evaluated typhoon disasters based on statistical relationships between the wind forces of landfalling typhoons and both casualties and economic damages (Fan and Liang, 2000; Qian et al., 2001). Disasters related to local extreme rainfall over land from typhoons have also been investigated. Tao (1980) pointed out that typhoons are the most intense rainfall systems, and the most extreme cases of heavy rainfall recorded in Chinese history were all produced by typhoons. Heavy rainfall and related secondary disasters such as flooding and mudslides are the primary disasters caused by typhoons (Chen and Ding, 1979). Zhang et al. (2010) compared the impacts of strong winds and rainstorms caused by typhoons and pointed out that the influence of rainstorms is more severe than that of strong winds. Furthermore, urban flooding becomes more severe with economic growth and urbanization in China (Xu et al., 2016; Duan et al., 2016; Shi, 2016). Consequently, local severe rainfall and related impacts of LTCs have increasingly become a focus of active research (Chen et al., 2004; Li et al., 2005; Dong et al., 2009; Nasrollahi et al., 2002; Wang et al., 2015).

The distribution of LTC precipitation includes inner-core rainfall, spiral rainbands, baroclinic instability rainfall, pre-TC squall line rainfall, and outer rainbands (Chen and Li, 2004). Chen et al. (2010) reviewed previous work on the torrential rainfall of LTCs and concluded that the factors that impact the intensity and distribution of torrential rainfall of landfalling typhoons include moisture transportation, extratropical transition, interactions between typhoons and monsoon troughs, orographic effects (i.e. land-surface processes), mesoscale convection within typhoons, and boundary energy transportation. Nevertheless, a typhoon's track is the most important element determining the distribution of torrential rain in operational forecasting and research (Xie and Zhang, 2012; Munsell and Zhang, 2014). Vertical wind shear (VWS) associated with landfalling typhoons is another key factor in determining the asymmetric distribution of typhoon rainfall (Gao et al., 2009); a certain magnitude of VWS can make the typhoon structure slant and cause rainfall maxima to occur on the left flank in the downshear direction (Jones, 1995; Frank and Ritchie, 1999). In addition, the direction and magnitude of VWS changes persistently with the asymmetric evolution of diabatic heating and upper-level winds (Li et al., 2015). Interactions between typhoon circulation and topography also play a key role in the asymmetric distribution and enhancement of rainfall (Lin et al., 2001; Li et al., 2003; Dong et al., 2009; Chih et al., 2015), and orographic effects on the enhancement of typhoon rainfall can be estimated using an idealized one-dimensional model (Smith, 1979; Xie and Zhang, 2012). The outer rainbands of a TC are generally the result of interactions between the outer circulation of the TC and mid-latitude weather systems (Tao et al., 1979; Jiang, 1983; Cong et al., 2011; Galarneau et al., 2010); however, dispersion of disturbed kinetic energy can generate TC outer rainbands in the mid-lower-latitude regions (Luo, 1994; Chen et al., 2002; Huang et al., 2014).

The intensity and distribution of typhoon rainfall result from the interactions between multi-scale systems because typhoon vortices are non-linear, complex structures (Luo, 2005; Teng et al., 2009; Luo et al., 2010; Moore et al., 2013). To date, no model can completely predict all distribution modes of typhoon rainfall. For instance, pre-TC squall line rainfall does not occur in all typhoons (Meng and Zhang, 2012). However, the intensity and distribution of typhoon rainfall are closely related to local topographic features, which increase the complexity of predicting the intensity and distribution of typhoon rainfall. Therefore, study of the local characteristics and related dynamics of landfalling typhoon rainfall may be beneficial for understanding and evaluating local severe rainfall.

Typhoon Soudelor (2015) produced heavy precipitation in the south and southeast of Zhejiang Province; the area that received above 300 mm of rainfall covered more than 8000 km^2. This amount of heavy rainfall over the Wenzhou and Taizhou regions of Zhejiang Province has a recurrence interval of 100 years. The geological disasters and flooding that resulted from the extreme precipitation of Soudelor led to 14 fatalities and over 8 billion CNY in direct economic losses. According to previous studies, the distribution of typhoon rainfall impacting Zhejiang Province included inner-core rainfall, spiral rainbands that extended 300–500 km from the center of the TC, frontal rainfall (baroclinic rainfall) induced by interaction between the northern (northwestern) circulation of the typhoon and the mid-latitude trough, and local orographic rainfall that resulted from interaction between typhoon circulation and local topography (Zhu et al., 1992). The local extreme accumulation of rainfall of Soudelor is distinct from that of other historical typhoons in terms of distribution and intensity, with the exceptional feature of maximum rainfall occurring around mountains.

2. Data description and TC case overview

Data utilized in this study include precipitation, the u and v components of wind at 10 meters, sea level pressure, surface pressure, relative humidity, temperature, and dew point temperature at 2 meters from mesoscale observational sta-

tions, Doppler radar reflectivity, FY2E stationary satellite infrared nephograms, the best-track dataset from the Shanghai Typhoon Institute of the China Meteorological Administration, and the final analyses of the Global Forecasting System (GFS) of the National Center for Environmental Prediction.

Typhoon Soudelor formed at 160.7°E, 13.7°N at 0000 UTC 30 July 2015 and translated north-northwestward, maintaining super-typhoon intensity (maximum sustained winds greater than or equal 51.0 m s^{-1}) for 66 h. Soudelor made its first landfall at Hualian, Taiwan Province at 2040 UTC 7 August 2015 while at severe typhoon intensity (maximum sustained winds up to 48 m s^{-1}). After the TC turned from southwestward from west-northwestward in the Taiwan Strait, a second landfall occurred at Putian, Fujian Province at 1410 UTC 14 August 2015 with maximum sustained winds of 48 m s^{-1} and minimum sea-level pressure of 970 hPa around the center. Subsequently, Soudelor translated westward in central Fujian Province into Jiangxi Province, and then turned northward across Anhui Province and moved into the East China Sea from central Jiangsu Province. Finally, Soudelor dissipated over the sea south of the Korean Peninsula (Figure 1).

Figure 1a shows that the track of Soudelor presents a quasi-circular movement from its landfall in Taiwan to its movement into the East China Sea across Jiangsu Province, which favored prolonged rainfall and production of heavy precipitation, and ultimately resulted in once-in-a-century torrential rainfall in the local regions of Taizhou and Wenzhou City in Zhejiang Province, China (Figure 2a). Soudelor began to decay from its landfall on Taiwan at severe-typhoon strength (maximum sustained surface winds greater than or equal to 41.5 m s^{-1}). It weakened slightly to typhoon strength as it translated over the Taiwan Strait, and then further decayed to a severe tropical storm, a tropical storm, and then a tropical depression in Jiangxi Province, Anhui Province and Jiangsu Province, China, respectively until rainfall ceased over Zhejiang Province (Figure 1b).

Figure 2a shows the precipitation accumulated during the rainfall period associated with Typhoon Soudelor in Zhejiang Province (from 0000 UTC 7 to 0000 UTC 11 August 2015). The distribution of precipitation clearly consisted of three regions. The first was located in the coastal region from northeast of Fujian Province to Wenzhou City, Zhejiang Province, and was influenced by the primary circulation of Soudelor with the longest rainfall time and maximum precipitation (rainfall region A in Figure 2; hereafter referred to as region A). The second was located in the region of Taizhou and Ningbo cities, Zhejiang Province, and resulted from the latitudinally orientated cloud band in the northeast quadrant of the TC that formed because of the expansion of the TC's broken rainbands (rainfall region B; hereafter referred to as region B). The third rainfall region was located in central Jiangsu Province and resulted from interaction between the outer circulation of the TC and the mid-latitude westerly trough. Furthermore, comparison of the rainfall distribution of the TC with topography shows that the heavy rainfall center is closely related to the locations of mountaintops. All heavy rainfall accumulation centers where Typhoon Soudelor produced rainfall in Zhejiang Province are in agreement with the centers of topographic height, except for the rainfall in central Jiangsu Province.

3. Dynamics of Local Severe Rainfall of Typhoon Soudelor

3.1 The stage characteristics of local severe rainfall of Typhoon Soudelor

Three kinds of typhoon precipitation occur in Zhejiang Province (Zhu et al., 1992; Wang, 2013). The first is the a priori precipitation at the southeast coast line and northwest mountains of Zhejiang Province, and is induced by interaction between the outer circulation of the typhoon and the weak cold air from the mid-latitude weather system, and is influenced by orographic enhancement effects on local severe rainfall before the typhoon makes landfall when it is located over the sea to the east of Taiwan Province, China. The second kind of rainfall is modulated by the typhoon's primary circulation with heavy rainfall centers over the Yandang Mountains, Siming Mountains, and Tianmu Mountains in Zhejiang Province, although rainfall distribution differs slightly because of the varying tracks and sizes of typhoons. The remnants of typhoon vortices after landfall can regenerate when connected to the transportation of warm moisture from the sea or the southwesterly jet and result in local severe precipitation in the third kind of rainfall. The rainfall distribution associated with different typhoon tracks shows that landfall in the middle to northern part of Fujian Province with westward or northwestward inland translation will generate the heaviest rainfall in Zhejiang Province. The disasters caused by local severe rainfall from Typhoon Soudelor were among the most severe of such events. Therefore, it is necessary to demonstrate the distribution and stage characteristics of this TC to further analyze the dynamic processes associated with this local severe rainfall.

The rainfall induced by Typhoon Soudelor can be divided into four stages based on the hourly rainfall distribution in East China. The first stage began from 0000 UTC 7 August 2015 and ended at 1200 UTC 7 August 2015 with the center of the TC located over the sea east of Taiwan; the weak rainfall occurred in the southeastern coastal regions of Zhejiang Province in this stage resulted from the outer circulation of Typhoon Soudelor. Both the rainfall intensity and accumulated precipitation in the second stage reached maxima in Zhejiang Province because of the impact of the pri-

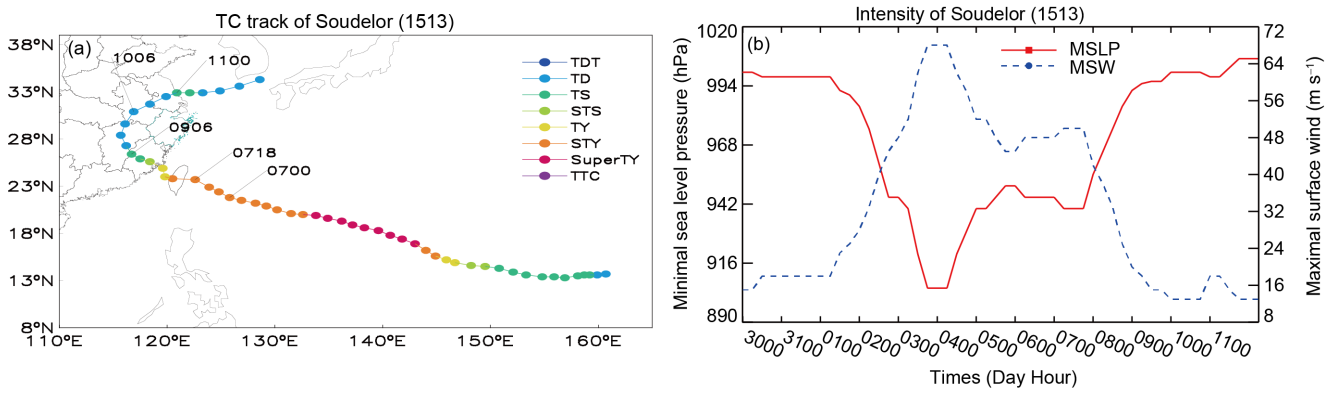

Figure 1 TC track (a) and intensity (b) of TC Soudelor (1513); red solid line denotes the minimal pressure at the TC center; blue dashed line indicates the maximum wind speed of the TC (0300 indicates 0000 UTC 3 August 2015, the rest likewise; TDT, TD, and TS represent tropical depression turbulence, tropical depression, and tropical storm, respectively in (a)).

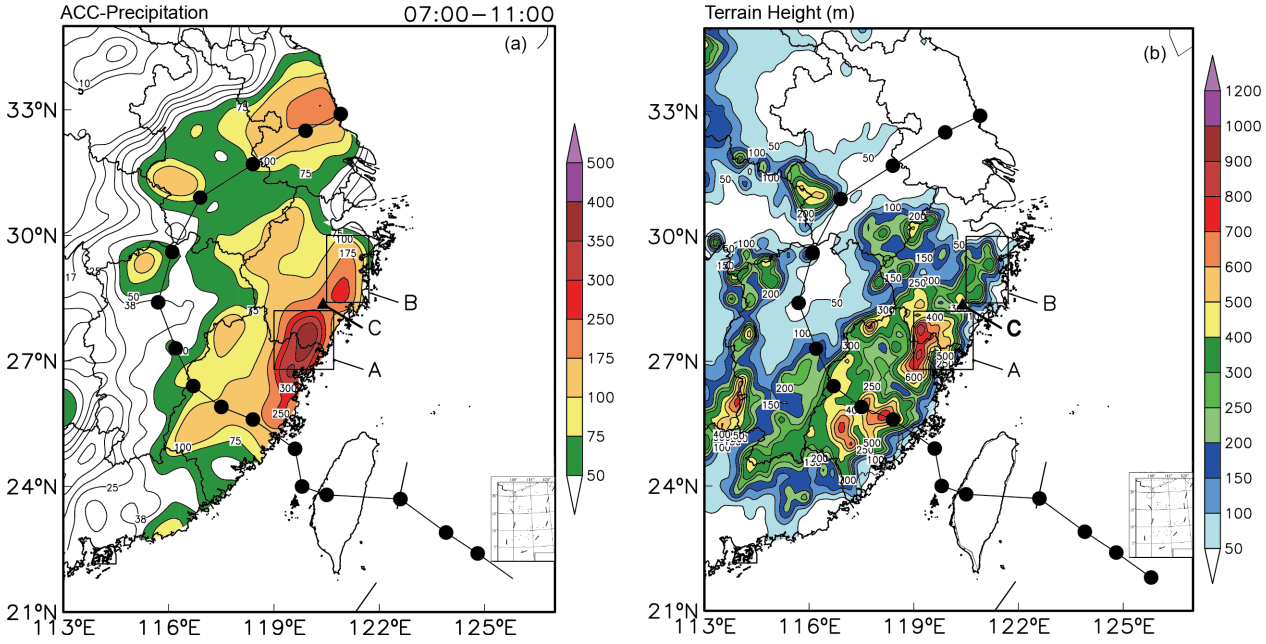

Figure 2 Accumulated precipitation (mm) between 0000 UTC 7 and 0000 UTC 11 August 2015 (black dotted line denotes TC track) (a) and terrain height (m) (b) in the Huadong District of China.

mary circulation of Soudelor as well as the longer-lasting duration of heavy rainfall from 0713 UTC 9 August to 0600 9 August 2015 when the TC made landfall in Fujian Province and translated westward over land. As Soudelor moved northward in Jiangxi Province in the third stage (from 0700 UTC 9 August to 0600 10 August 2015), the TC intensity decayed significantly, and its structure became asymmetric with the primary rainbands breaking and shifting to the northeast quadrant of the TC, which led to the occurrence of local severe precipitation in the Taizhou and Ningbo regions of Zhejiang Province. In the fourth stage (from 0700 UTC 10 to 0000 UTC 11 August 2015), the TC gradually turned from northward to northeastward, and the cloud clusters with the greatest convection shifted northward as TC intensity continuously decreased. As a result, the major rainband moved to the middle and eastern parts of Jiangsu Province, and rainfall in Zhejiang Province ended as the convective cloud bands moved to the East China Sea.

To further characterize the rainfall distribution of Soudelor in Zhejiang Province, time series of the evolution of area-averaged precipitation across all of Zhejiang Province and the principal severe rainfall regions were calculated (Figure 3). The region of Zhejiang Province for calculating area-averaged rainfall is defined from 118°E to 123°E and from 27°N to 30.5°N, and contains 2082 mesoscale observational stations. Region A, which covers Wenzhou City and includes 423 mesoscale observational stations, is defined from 119°E to 120.7°E and 26.8°N to 28.2°N, and region B, which covers Taizhou and Ningbo cities and has 622 mesoscale observational stations, is defined from 120.5°E to 121.7°E

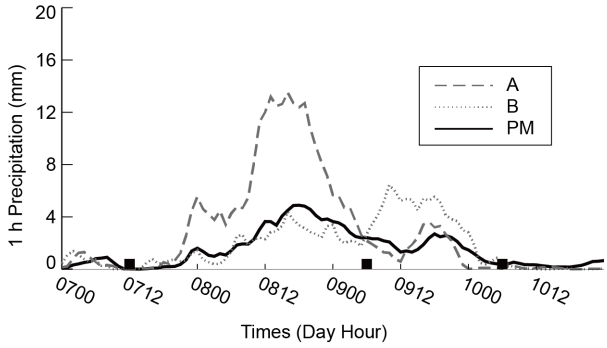

Figure 3 Evolution over time of area-averaged precipitation (mm) in Zhejiang Province (PM, solid line), region A (dashed line) and region B (dotted line). The four precipitation phases are divided by black squares along the *X*-axis (0700 indicates 0000 UTC 7 August 2015, the rest likewise).

and 28.4°N to 30.0°N. All regions were interpolated into horizontal grids of 5 km×5 km using a Kriging interpolation method. The average value at each time point for each region was calculated by dividing the sum of the precipitation at each grid point by the total number of grid points. Figure 3 shows the rainfall features in different stages. In the first stage, TC rainfall increased and then decreased rapidly, ending at 1200 UTC 7 August 2015, which differed from the previous TC rainfall mode (Zhu et al., 1992; Wang, 2013) in that rainfall intensity was weak without interaction between outer circulation of the TC and mid-latitude cold air. With the landfall of the TC in Taiwan in the second stage, the accumulated precipitation increased significantly; notably, the fastest rise of accumulated rainfall occurred in region A, although the rainfall intensity presented small fluctuation as the TC translated over Taiwan and the Taiwan Strait with a curved track that propagated southwestward and then turned northwestward. Wenzhou City and neighboring regions were affected by the principal rainbands of the TC as Soudelor made its second landfall in Fujian Province; about 300 km from the center of the TC, rainfall intensity increased rapidly and reached a maximum at 1600 UTC 8 August 2015. The rainfall in this stage ended at 0600 UTC 9 August 2015 when the TC translated farther inland, and intensity and rainfall rate decreased dramatically. The rainfall intensity variation in the second stage shows that the precipitation in this stage was attributed to rainfall in region A. Meanwhile, there were multiple convective rainbands in the northeast quadrant because of the northward propagation of disturbed energy of the typhoon (Corbosiero et al., 2006; Li et al., 2007; Hall et al., 2013), which resulted in some precipitation in the north of the TC's circulation (region B) with much weaker intensity than in region A. In the third stage, the intense rainfall shifted from the middle and south of Wenzhou City to the region of Taizhou and Ningbo cities (region B) when Soudelor turned from westward to northward as it entered Jiangxi Province. Rainfall intensity in region B increased significantly. However, the rainfall rate in region A remained weaker than that of region B. As the rainfall bands of Soudelor shifted northeastward, the rainfall intensity in Zhejiang decreased, which represented the fourth stage of rainfall. Precipitation in regions A and B decreased significantly, and the weak rainband along coastal region of Zhejiang Province shifted to the coastal islands and Zhoushan City as the TC moved further eastward, which marked the end of rainfall in Zhejiang Province.

Figure 4 shows composites of accumulated precipitation in each rainfall stage obtained by calculating the sum of rainfall with time at each grid point for each stage. Little rainfall occurred over Yandang Mountain of Wenzhou City and Siming Mountain of Taizhou and Ningbo cities in the first stage. Because the distance between the center of the TC and the rainfall area was over 800 km, precipitation in this stage represents a category of rainfall far from the typhoon (RFT, Figure 4a). In the second stage (Figure 4b), TC precipitation occurred in the region from northeast of Fujian Province to southeast of Zhejiang Province, with the maximum precipitation occurring in the middle-southern region of Wenzhou City. This precipitation was the most intense and covered the largest area of all stages. The orientation of precipitation distribution in this stage is in agreement with the local coastal topography, which suggests a close relationship between the intense TC rainfall and local topographic features. The rainband then shifted further to the north and was oriented latitudinally with two dominant rainfall centers around Taizhou and Ningbo cities of Zhejiang Province (region B) and the middle-west part of Anhui province, respectively, which demonstrates that the spiral cloud band had broken as the primary circulation of the TC extended northward. The phenomenon of broken rainbands was captured by the hourly evolution of radar reflectivity. The reflectivity band in the second stage gradually split into multiple intense cloud cluster centers as the spiral band evolved toward the northeast quadrant of the TC in the third stage (figures omitted). The principal rainfall areas shifted northward in the mid-eastern regions of Jiangsu Province and east over the East China Sea in the last stage of rainfall, which is consistent with the distributions of intense radar reflectivity bands over that area. There was little rainfall (less than 5 mm) in the coastal regions from Taizhou to Ningbo city and gradually ended.

The above analysis of the evolutions of hourly rainfall distribution and area-averaged precipitation shows that the rainfall in Zhejiang province that resulted from Typhoon Soudelor can be divided into four distinct stages. Therefore, composite analysis of each stage of rainfall will be utilized to further investigate the physical processes responsible for the formation of rainfall in each stage.

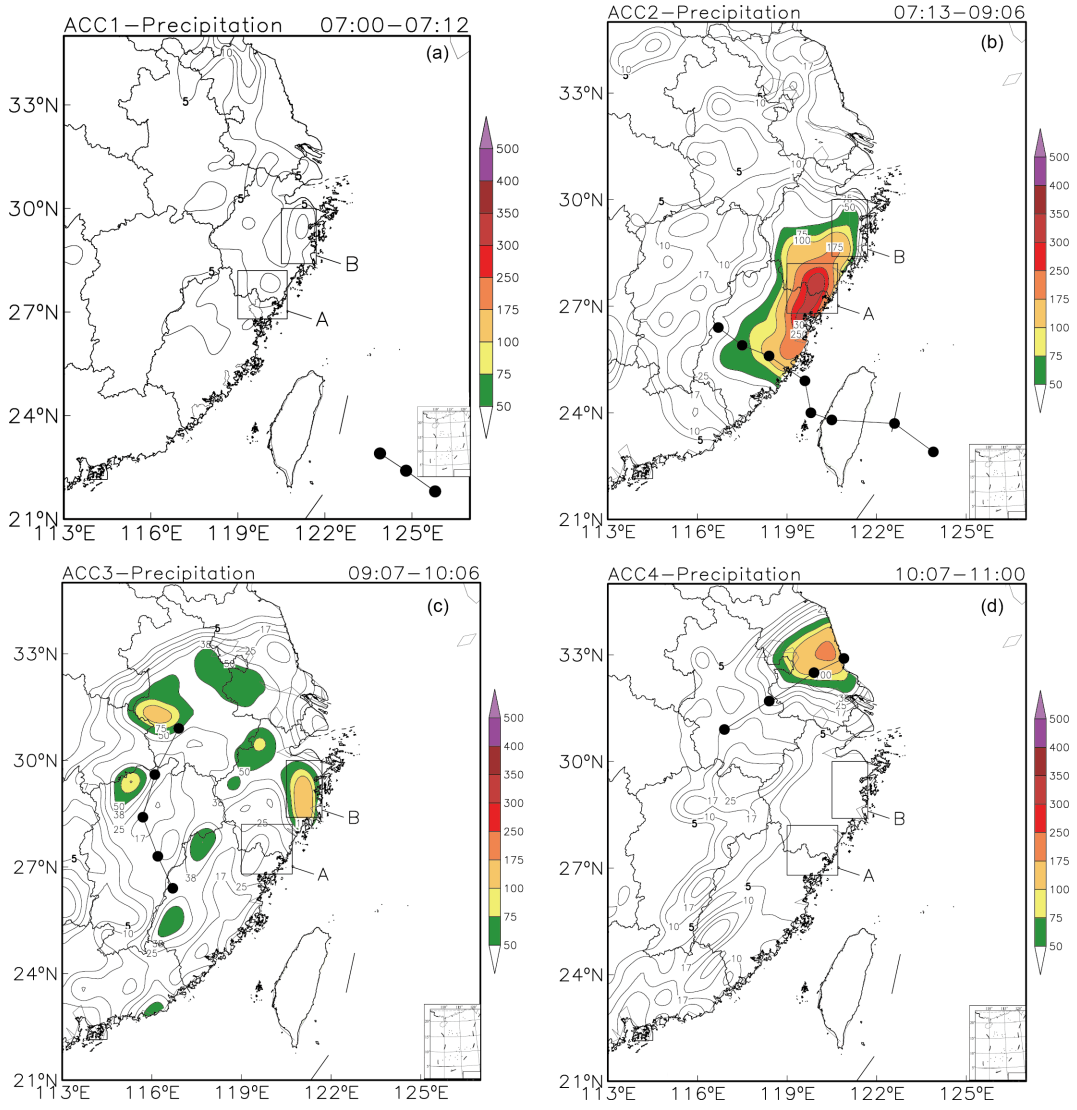

Figure 4 Precipitation (mm) in each rainfall phase of TC Soudelor (1513). Shading denotes rainfall greater than 50 mm.

3.2 Relationship between the formation in the first stage and RFT

Chen (2007) provided definitions of RFT including (1) the precipitation that occurs outside of the typhoon circulation and (2) there is coherent intrinsic relation between the typhoon and RFT that separates the rainfall within typhoon circulation from the RFT. RFT is a category of local severe rainfall that occurs outside of the typhoon's principal circulation with a distance greater than 800 km from the typhoon's center, and results from the interaction between the outer circulation of the typhoon and mid-latitude weather systems (Tao et al., 1979). There is another category of RFT in subtropical regions (south of 35°N) that results from local vortices generated by the dispersion of disturbed kinetic energy of the typhoon located distant from the RFT (Luo, 1994; Chen et al., 2002; Huang et al., 2014). The precipitation that occurred in Zhejiang Province in the first stage was RFT according to this definition because Soudelor was located over the sea east of Taiwan, and the distance between the rainfall area and the typhoon center was over 800 km. Nevertheless, the intensity of the RFT in Zhejiang Province, only 10 mm at most, was far less than the RFT defined by Chen (2007) and Tao et al. (1979).

Figure 5 shows a composite of surface winds in each stage of rainfall. Northeasterly winds prevailed in regions A and B with the magnitude of the whole wind velocity less than 8 m s^{-1} (Figure 5a). The local convergence in region B was greater than that in region A, which caused more intense local convection in region B than in region A, in addition to the warm, moist easterly wind from the East China Sea that resulted in more precipitation in region B than in region A (Figure 4a). Figure 6 shows the evolution of wind over time at different pressure levels for regions A and B. North-

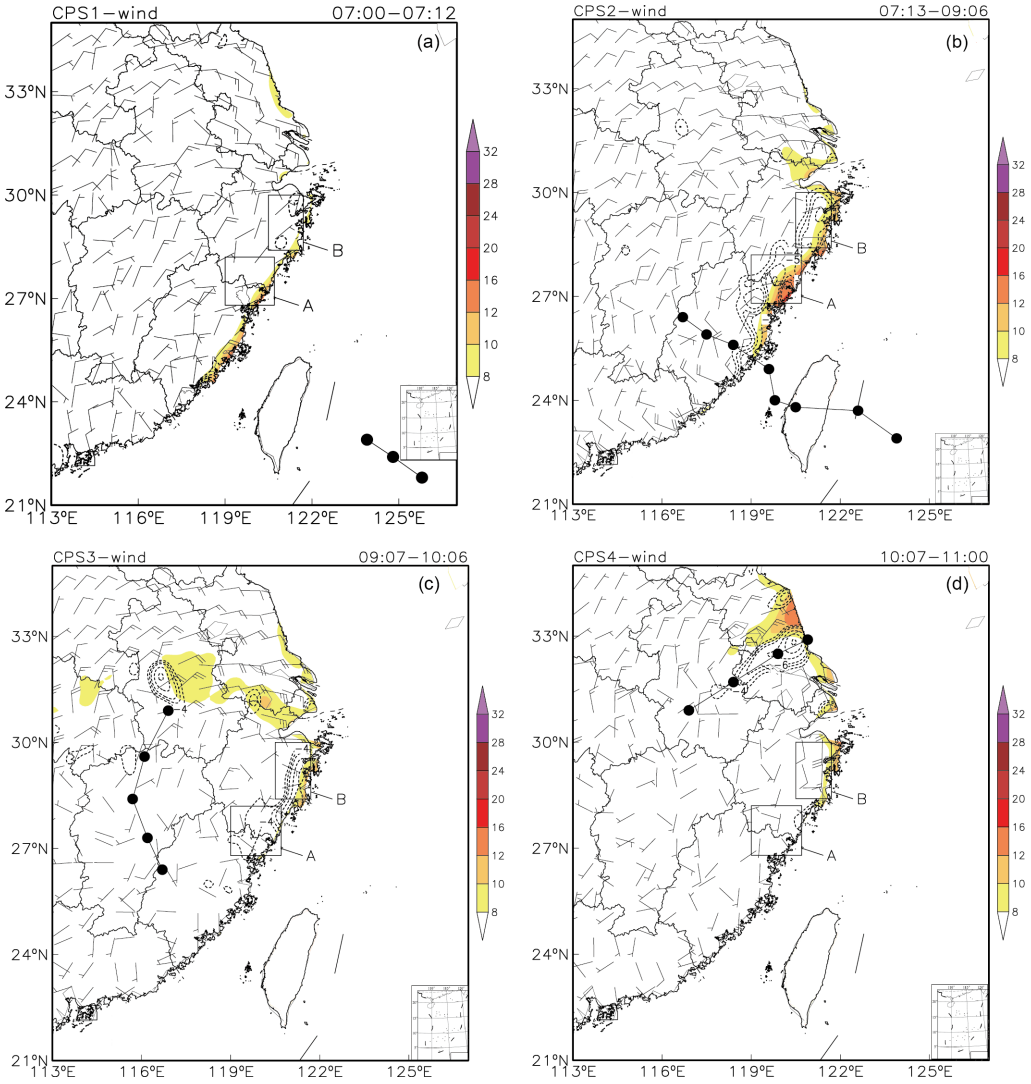

Figure 5 The evolution of composite observed station wind velocity (full bar=10 m s^{-1}, shading denotes wind velocity over 8 m s^{-1}) during different TC rainfall phases ((a) phase I, (b) phase II, (c) phase III, (d) phase IV dotted contours denote divergence with units of 10^{-5} s^{-1}).

easterly winds dominated region A below 700 hPa, and the prevailing wind shifted from northeasterly to easterly within 1000 to 700 hPa in the first stage. In contrast, easterly winds prevailed below 700 hPa in region B. The wind velocity in both regions was relatively low, with speeds less than 8 and 12 m s^{-1} below 850 and 700 hPa, respectively. The evolution over time of area-averaged vertical velocity in region A, B, and Zhejiang Province (Figure 7) shows that the magnitude of vertical velocity in region A was comparable to that in Zhejiang Province in the first stage, and was lower than that in region B. Furthermore, the magnitudes of vertical wind velocity in all three regions were relative small, with values less than 0.3 h Pa s^{-1}. All of the above characteristics show that precipitation in the first stage resulted from relatively weak convection.

Smith (1979) proposed a one-dimensional idealized model to estimate the rainfall rate induced by topography (eq. (1)):

$$\begin{cases} R_{\mathrm{T}} = -\vec{S}\cdot\int_0^{\infty}\vec{V}\dfrac{\mathrm{d}\rho_{\mathrm{w_s}}}{\mathrm{d}z}\mathrm{d}z, \\ \vec{S} = \nabla\cdot H \end{cases} \quad (1)$$

where R_{T} is the rainfall rate of the orographic effect in units of mm, ρ_{ws} is the saturated vapor density, $\vec{S}$ is the topographic gradient, H is topographic height, and $\vec{V}$ represents the surface wind vector. Because the change of wind velocity within the boundary layer is small, and because the saturated vapor density is equal to zero at the top of the boundary layer, eq. (1) can be simplified as (Xie and Zhang, 2012):

$$R_{\mathrm{T}} = \left(u\frac{\partial H}{\partial x} + v\frac{\partial H}{\partial y}\right)\times r_{\mathrm{s}}(0)\times\rho_{\mathrm{air}}(0), \quad (2)$$

where, $r_{\mathrm{s}}(0)$ and $\rho_{\mathrm{air}}(0)$ indicate the surface water vapor mixing ratio and air density, respectively; u and v represents the zonal wind component and the meridional wind component, respectively.

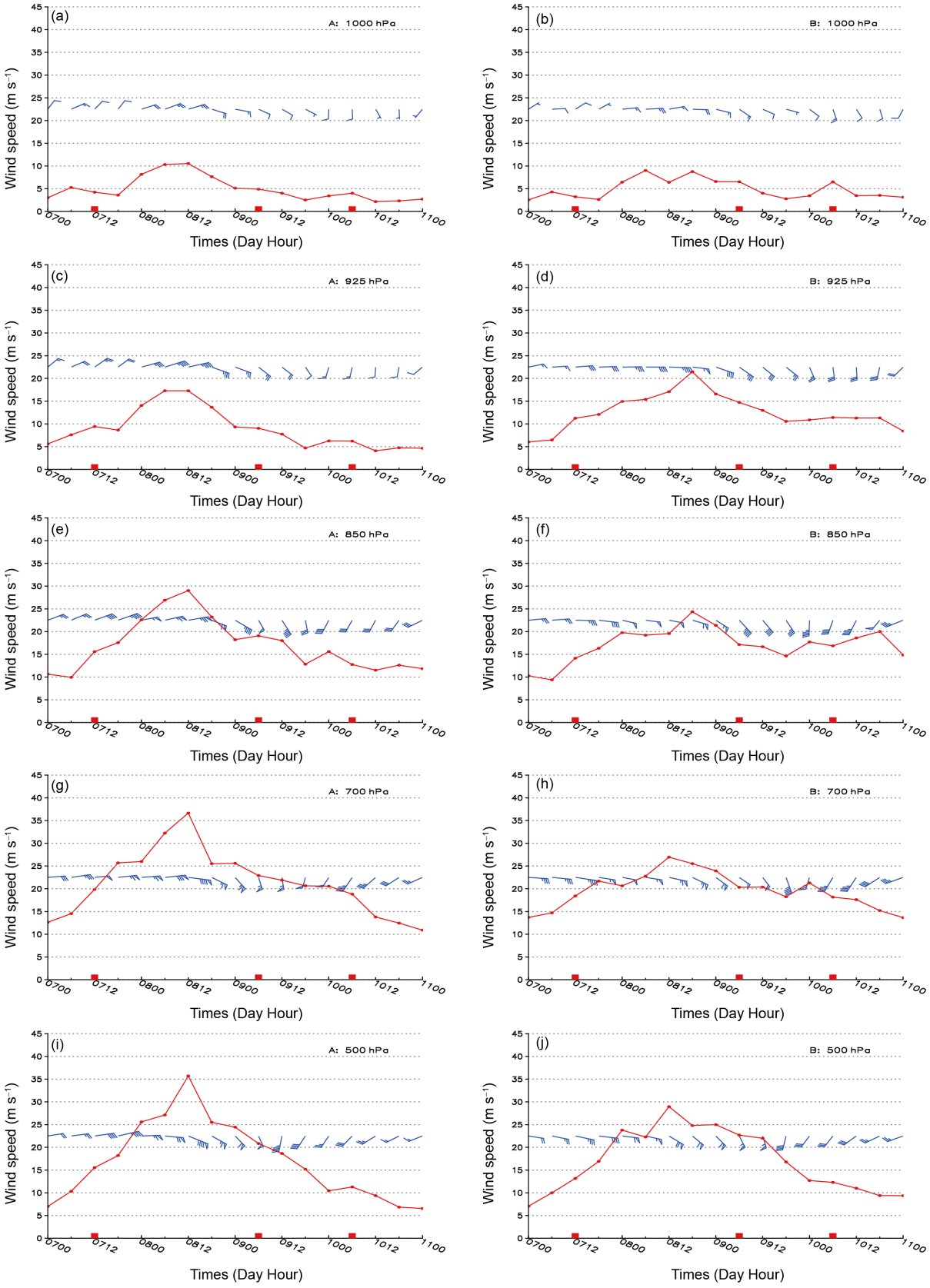

Figure 6 Evolution over time of area-averaged velocity vectors and whole wind velocity (m s^{-1}) in regions A ((a), (c), (e), (g)) and B ((b), (d), (f), (h)). Red solid squares separate each precipitation phase; black solid triangles indicate the two landfall times, in Taiwan and Fujian Province, respectively; abscissa is the same as in Figure 3.

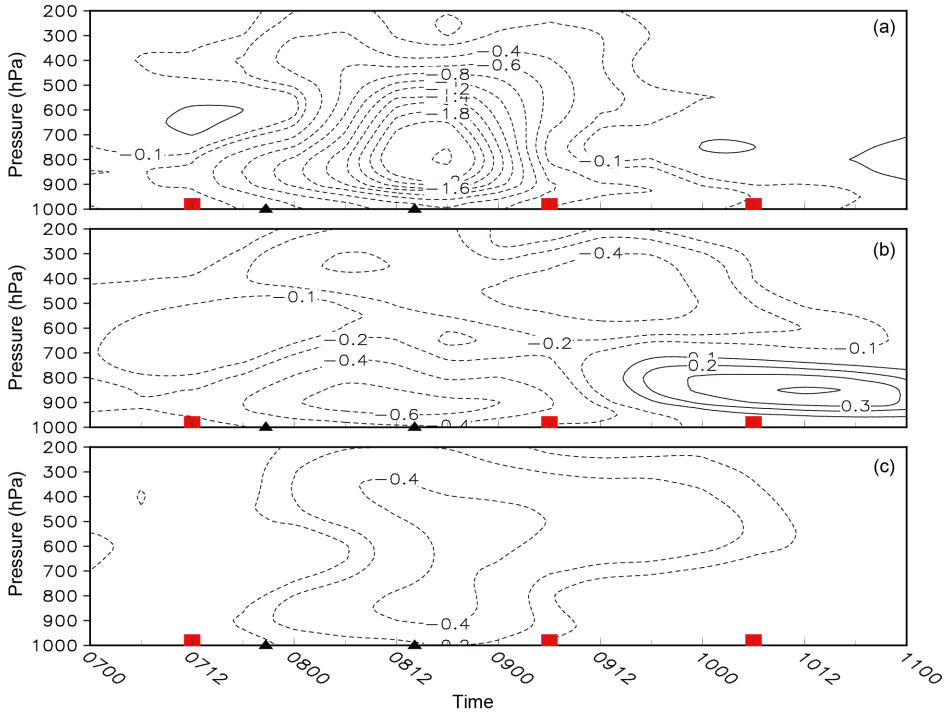

Figure 7 Time-pressure vertical cross-section of area-averaged vertical velocity (Pa s^{-1}) over region A (a), region B (b), and Zhejiang Province (c). Solid squares separate the four rainfall phases; solid triangles denote the times of landfall in Taiwan and Fujian provinces, respectively; abscissa is the same as in Figure 3.

Eq. (2) demonstrates that R_T is positively proportional to the horizontal wind velocity, topographic gradient, and water vapor density near the surface. In other words, greater horizontal wind velocity, topography gradient, or vapor content per unit volume corresponds to larger orographic effects on the enhancement of rainfall.

Figure 8 shows the composite distribution of R_T in each stage of rainfall, calculated based on mesoscale surface observations in East China, including wind direction and velocity at 10 m, relative humidity at 2 m, water vapor pressure, surface pressure, and topographic height. In the first stage, the value of R_T is between 5 and 10 mm, which is comparable to observations, and indicates that rainfall of this stage represented distant rainfall that resulted from weak convection caused by interactions between lower-tropospheric wind and local topography.

Therefore, the interaction between the outer circulation of Soudelor in the lower troposphere and local topography in the first stage was the predominant factor leading to the distant rainfall of the TC during the first stage based on comparison of wind directions and R_T distribution. Moreover, easterly wind is more favorable to local convection and precipitation in coastal regions because the orthogonal component of the easterly direction is greater than that of the northeasterly direction to the southwest–northeast-oriented coastal topography of Zhejiang Province.

3.3 Effects of the interactions of multiple factors on the dynamics of local severe precipitation in the second stage

Analysis of Figure 3 above shows that the area-averaged rainfall in region A increased significantly over time from about 3 h before landfall of Soudelor on the island of Taiwan (1800 UTC 7 August 2015) and reached a maximum as the TC made its second landfall in the central coastal region of Fujian Province. Then, the area-averaged rainfall decreased gradually as the TC translated further inland. The mean rainfall rate in region A was far greater than that in region B and Zhejiang Province, which indicates that the most intense rainfall in the second stage occurred in region A. Therefore, the mechanism of severe rainfall in the second stage has been explored in terms of the interactions of multiple factors involving the principal circulation of the TC, local topography, and synoptic conditions.

The radius at the maximum velocity of the TC (r_m) is closely related to the eyewall and spiral cloud bands around eyewall, which notably impact the rainfall distribution within the eyewall of the TC (Rogers et al., 2009). In the second stage, the severe precipitation that occurred in regions A and B represented some of the principal rainband rainfall of the TC because the distance from the TC center to both regions was between 300 and 500 km. The evolution of r_m over time (Figure 9), calculated using the best track data of the Joint Typhoon Warning Center (JTWC) of the United States, was

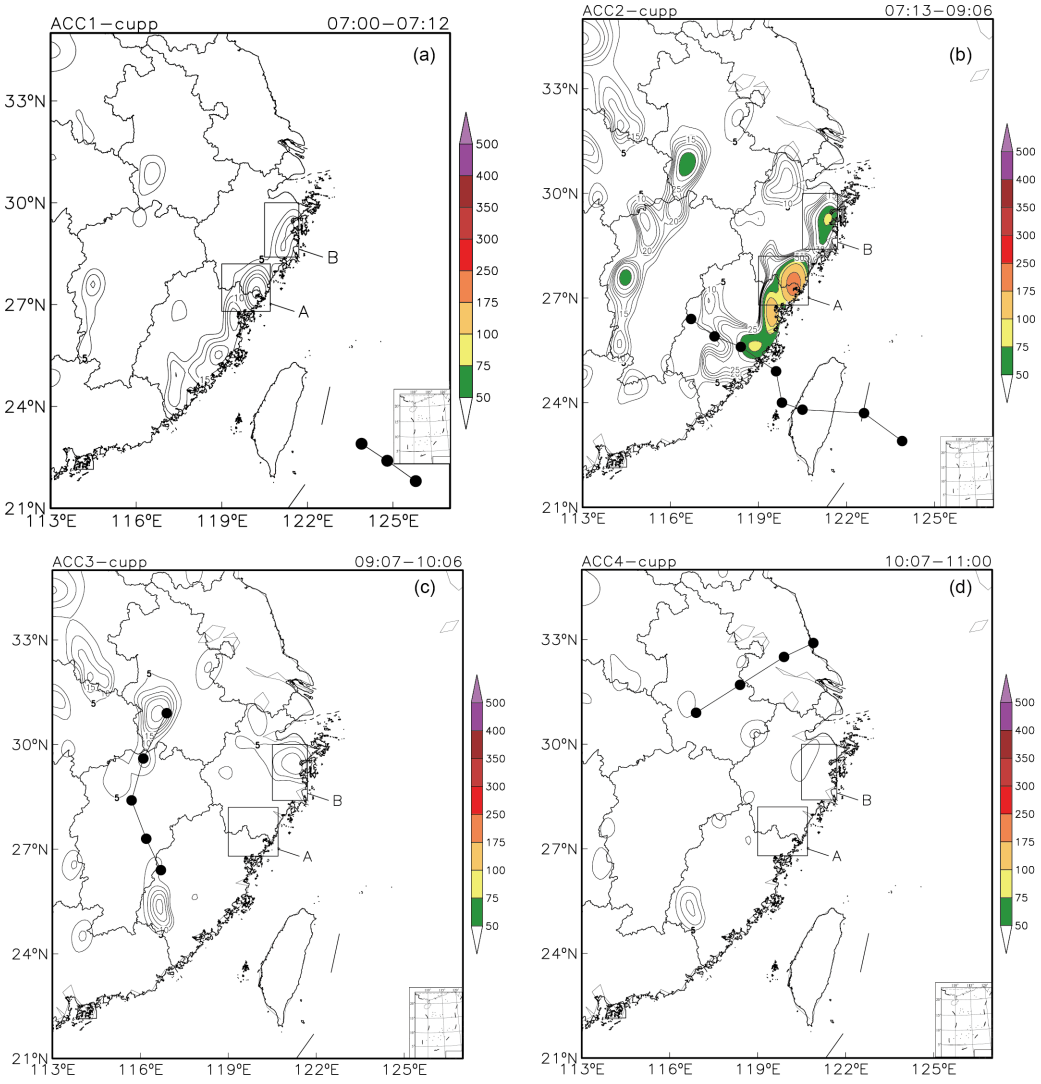

Figure 8 Distribution of R_T (mm) in the Huadong District of China. Shading indicates values greater that 50 mm; solid dotted line denotes the TC track in each rainfall phase.

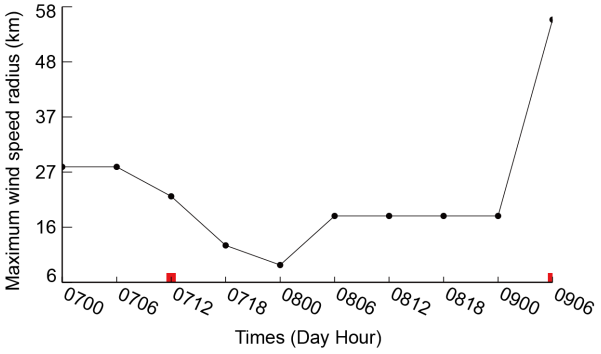

Figure 9 The maximum wind speed radius (km) of TC Soudelor from 0000 UTC August 7 to 0000 UTC August 11, 2015. Abscissa is the same in as Figure 3.

employed to investigate the relationship between r_m and severe precipitation in the second stage. The value of r_m decreased remarkably during the transition from the first stage to the second stage of rainfall, and reached a minimum of about 10 km at 0800 UTC 8 August. Subsequently, r_m grew and remained around 13 km until the end of the second stage of rainfall. Then, r_m increased rapidly over time in the third stage.

Based on comparison of the evolution of r_m and area-averaged rainfall in region A in the second stage (Figure 10), an opposite phase variation occurred, which implies that the fluctuation of r_m reflected the tendency of local severe precipitation within the principal rainband of Soudelor 300–500 km from the TC center.

Figure 4b shows that the precipitation distribution of the typhoon was very asymmetric; extreme rainfall above 50 mm was located almost entirely to the right of the TC track, and the maximum rainfall occurred in region A, which was 300 km from the TC center and was modulated by the principal rainband. Moreover, severe rainfall was localized;

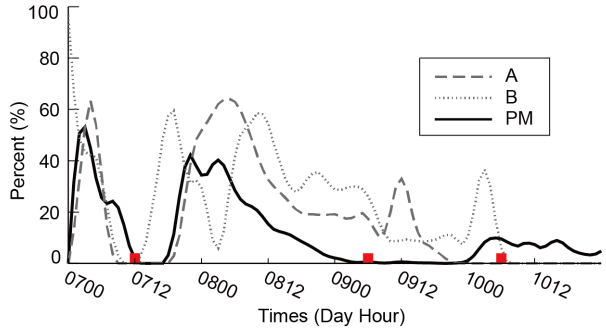

Figure 10 Time evolution of percent (%) of area-averaged R_T relative to observational precipitation for regions A and B, and for Zhejiang Province. Abscissa is the same as in Figure 3.

intense rainfall occurred over large mountains along the coast, and rainfall decreased rapidly inland, which indicates that the mountainous topography may have had dramatic impact on the rainfall distribution of the landfalling typhoon. Meanwhile, local convection developed asymmetrically in the outer rainbands in the direction parallel to the TC track. The asymmetric development of typhoon precipitation associated with local intense convection was closely correlated with the wind field in the lower troposphere and the interaction between wind and topography in the TC circulation (Chen et al., 2010). The local topography lifted the moist air to convection condensation level (CCL) and rainfall occurred; however, the orthogonal component of upslope flow over the local topography sped up the vertical velocity of the rainfall convection system, which led to further development of local convection and the growth of the asymmetric distribution of local intense convection.

Figure 5b shows a composite image of the wind vectors and divergence at 10 m. The strong wind areas were located in the coastal regions from northeast of Fujian Province to southeast of Zhejiang Province, with the maximum wind velocity center located in region A where east-northeasterly winds prevailed in the second stage. In addition, surface convergence was most intense in region A, and both surface wind vectors and convergence declined sharply inland. This finding indicates that the development of local convection in the coastal mountainous regions from northeast of Fujian Province to southeast of Zhejiang Province can be attributed to two factors. One was the vertical shears of wind velocity and direction caused by the reduction of wind velocity induced by surface friction, which can result in local convergence; the other was the interaction between surface wind and topography, which can speed up near-surface vertical velocity through a lifting effect.

Figure 6 shows the changes of the wind velocity and direction in the lower troposphere. The wind direction shifted from northeasterly to east-northeasterly and then to southeasterly in region A, but from east-northeasterly to southeasterly in region B in the second stage. The wind velocity reached maxima before landfall of the TC in region A, but 4 h after landfall for region B. Intense wind could bring more water vapor to the rainfall regions, which would facilitate the enhancement of local severe rainfall, and is in agreement with maximum precipitation occurring in region A. Furthermore, the wind direction in region A in the second stage was predominantly easterly, which demonstrates that there is a correlation between easterly and local severe precipitation in this region because of the stronger component of the easterly winds orthogonal to the coastal mountainous topography of Zhejiang Province. As the wind direction shifted to southeasterly, starting around at 1800 UTC 8 August, precipitation decreased dramatically in region A (Figure 3). Analysis of the vertical upward motion closely related to the mid-lower wind field shows that the vertical upward motion in region A increased drastically in the second stage with maxima around the time of landfall of Soudelor in Fujian Province. For the whole troposphere, the primary vertical upward motion occurred below 500 hPa, with maxima occurring at pressure levels from 850 to 600 hPa, which indicates that convective development was restricted within the lower troposphere, and the intensity of the rainfall convective system was moderate. This phenomenon can be confirmed based on the radial-vertical cross-section of radar reflectivity from when the most intense precipitation occurred. The vertical extension of the maximal reflectivity is concentrated in a small area to the east of the rainfall region with smaller height and discontinuous distribution, and the intensity of radar reflectivity was moderate overall (40–50 dbz, figures omitted). It follows from the analysis of area-averaged hourly rainfall rates (Figure 3) that the situations that resulted in local severe precipitation in Zhejiang Province were not short-term intense convective systems but resulted from the combined effects of multi-scale intense rainfall systems over a relatively long period. The reasons for the maintenance of intense rainfall over a long period of time are explored in Section 3.6. Because the moderately intense convection of the spiral rainbands of Soudelor cannot explain the severe precipitation that occurred in the second stage, orographic effects must have played an important role in the intense rainfall process.

Figure 8b shows the distribution of the orographic rainfall rate R_T in the second stage. Because the rainfall regions were modulated by the principal circulation of the TC, with a smaller radius of maximum wind velocity (Figure 9), considerable growth of wind velocity (Figure 5b), and enhancement of local convergence, R_T increased remarkably, which resulted in a dramatic increase of the hourly rainfall rate (Figure 3). Although TC intensity decreased significantly as Soudelor translated farther inland, R_T still maintained a large value because the orthogonal component of the easterly winds to zonal mountains was large, with the rainfall regions modulated by the northern part of principal

circulation of the TC and warm moisture flow from the East China Sea. Consequently, the rainfall rate remained within 5 to 15 mm h^{-1} for over 24 h. Moreover, precipitation in the second stage lasted from 1200 UTC 7 August to 0600 UTC 9 August, or around 42 h in total, and the accumulated precipitation was far greater than normal for torrential rain.

The role of R_T in the total precipitation from Soudelor was investigated further by calculating the ratio of area-averaged R_T to area-averaged precipitation in region A, region B, and Zhejiang Province (Figure 10). The contribution of area-averaged R_T in Zhejiang Province to area-averaged total rainfall was 20%–40% within the first 12 h of the second stage, and then decreased rapidly; however, the contribution of R_T in regions A and B reached up to 60% with little fluctuation. In the transition period from the second stage to the third stage, the contribution of R_T, up to 60% of the total precipitation, reduced sharply as the TC translated farther inland. This analysis demonstrates that the interaction between TC circulation and local mountains played an important role in the formation of local torrential rainfall of this typhoon, with the contribution of R_T to total precipitation exceeding 50% in some rainfall periods.

From eq. (2), we know that R_T increases with the growth of the orthogonal component of the wind. Greater wind velocity corresponds to more rapid increase of R_T. Therefore, the R_T caused by easterly wind was most intense because the orientation of the topography from central Fujian Province to the southeastern coastal region of Zhejiang Province primarily runs north-south.

The above analysis indicates that the maintenance of a small radius at maximum wind velocity was favorable for the maintenance of local sustained rainfall in the primary spiral rainbands of the typhoon, and that local rainfall was then significantly enhanced by interactions between typhoon circulation and the local topography. Moreover, the maintenance of a small radius at maximum wind velocity and the corresponding rainfall intensity and distribution are closely related to vertical wind shear (Jones, 1995; Wong and Chan, 2004; Chen et al., 2006; Gao et al., 2009; Zhang and Tao, 2013; Tao and Zhang, 2014). Therefore, the relationships between local severe rainfall and two kinds of VWS were explored by calculating the evolution of azimuthal average VWS over time in the typhoon circulation region (TVWS) within 300 km from the typhoon center (Figure 11a) and environmental VWS (EVWS) 300–500 km from the typhoon center (Figure 11b). Figure 11 shows that the TVWS in the second stage shifted from northwesterly to east-southeasterly, and then turned to southwesterly clockwise. The magnitude of TVWS decreased to around 5 m s^{-1} from 8 m s^{-1} in the first stage, and remained at this level until the end of rainfall in the second stage, which is consistent with the results in Tao and Zhang (2015) that the intensity of VWS with magnitude below 6 m s^{-1} facilitates the maintenance and development of convection within the typhoon circulation. Meanwhile, the EVWS shifted from northwesterly to easterly, and then turned to southwesterly clockwise before the end of rainfall in the second stage with the reduction of intensity of TVWS from 8 to 2 m s^{-1}, and this intensity was maintained until the end of rainfall in the second stage. Thus, the small VWS was favorable to the maintenance of the intensity and structure of the TC, and represents a necessary condition to ensure the formation of local sustained severe precipitation in the second stage. Furthermore, Corbosiero and Molinari (2002) found that the most active convection in the outer rainband of a TC is typically located in the left flank in the downshear direction. In contrast, severe rainfall associated with Soudelor was located in the right flank of the easterly VWS in the second stage, which confirms the key role of local topography in the intensity and distribution of precipitation in the second stage.

Figure 12 showsthe distributins of the composite divergence and wind vector fields at 850 hPa (Figure 12a, c, e, g) and 200 hPa (Figure 12b, d, f, h) during different rainfall stages. Region A was modulated by the principal circulation of the TC with a strong easterly lower-level jet (LLJ), and the convergence area was located in the coastal region from central Fujian Province to central Zhejiang Province at 850 hPa. There was a weak divergence zone at the top of the TC

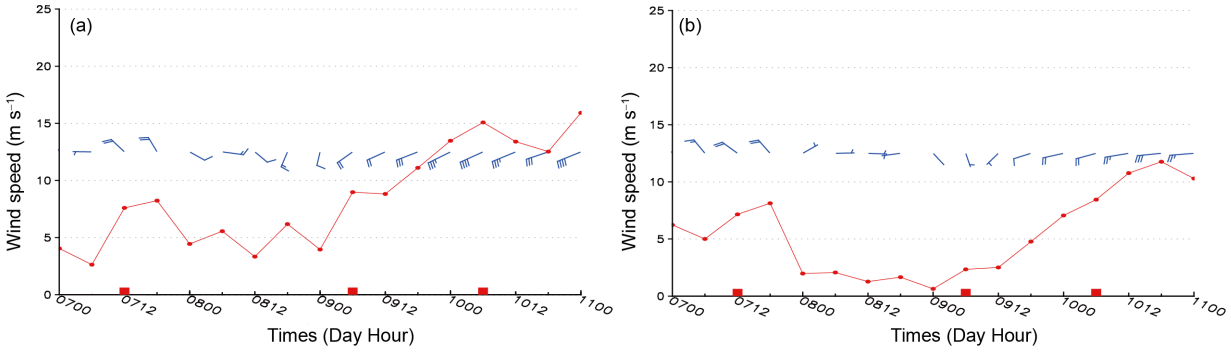

Figure 11 Vertical wind shear within the TC (a) and in the environment (b) for TC Soudelor from 0000 7 August to 0000 11 August 2015. Abscissa is the same as in Figure 3.

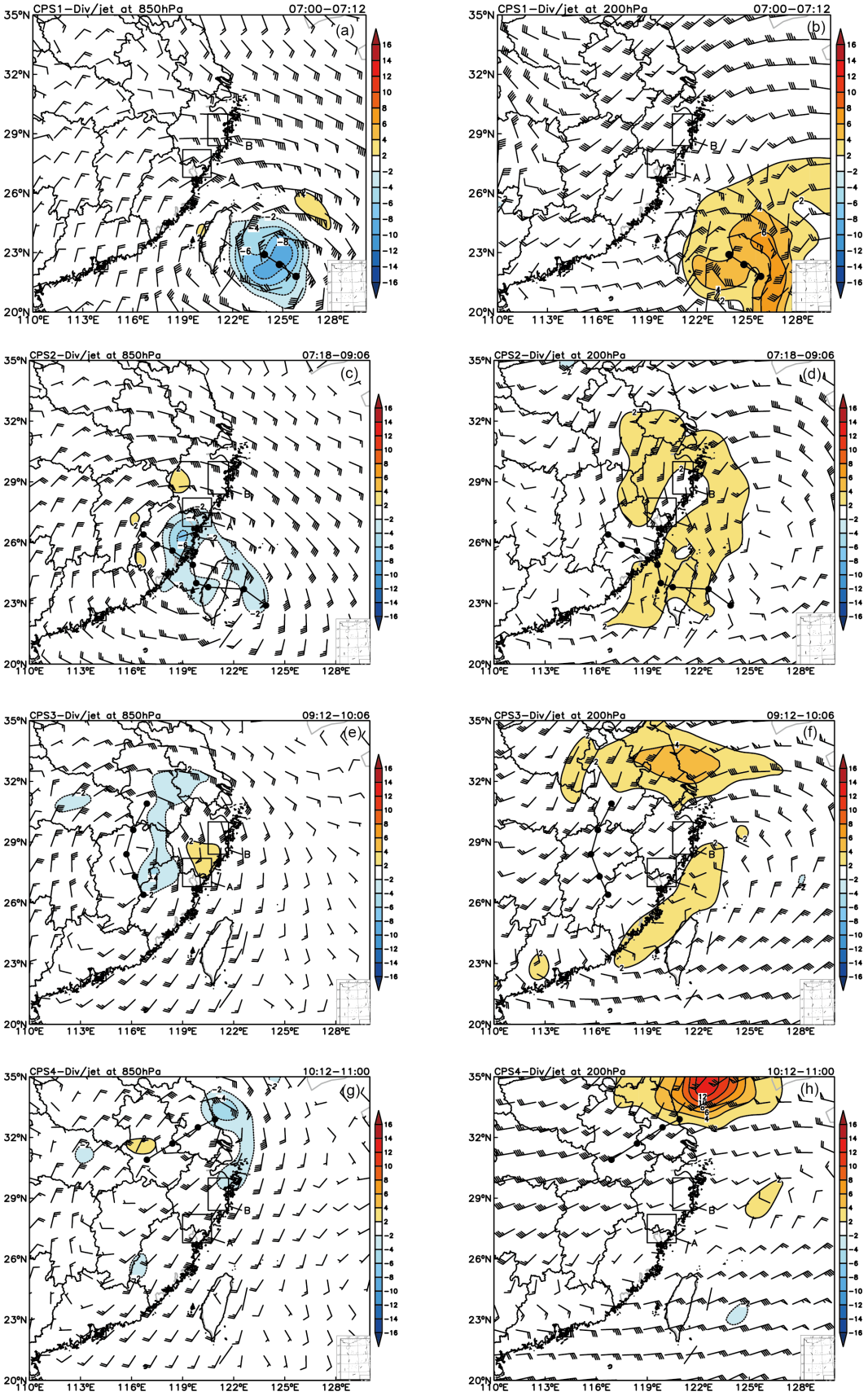

Figure 12 Composite of divergence (shaded, 1 e^{-5} s^{-1}) and wind vector field (full bar=10 m s^{-1}) at 850 hPa ((a), (c), (e), (g)) and 200 hPa ((b), (d), (f), (h)).

at 200 hPa. Meanwhile, the TC was influenced greatly by the VWS because of its small value (Figure 11). The stronger convergence zone occurred in the northeast quadrant of TC circulation in the upper troposphere (Figure 12d). This layout of divergence and wind vectors at lower and upper pressure levels was favorable for further development of convection near the surface. Consequently, the TVWS had important influence on the maintenance of convection activity in the lower troposphere in the rainfall regions during the occurrence of severe local rainfall of the typhoon. In particular, the weak VWS contributed to the maintenance of the relatively stable structure of the TC and sustained precipitation. At this time, Soudelor remained at typhoon or severe tropical storm strength in the second stage, and the radius of the maximal wind velocity barely changed, which was essential to the formation of local severe rainfall accumulation induced by the interaction of the principal circulation of the TC and local mountainous topography.

The above analysis shows that the maximum extreme precipitation induced by Soudelor in the second stage resulted directly from the interaction of the moderately intense principal circulation of the TC and local topography. The small change in the intensity and structure of TC circulation caused by the small VWS, which facilitated the maintenance and development of the stable primary rainband in region A, was another important condition for the extreme precipitation in the second stage.

3.4 The effect of typhoon structural changes on the northward shift of the precipitation center in the third stage

Analysis of Figure 3 reveals that the rainfall in region B increased rapidly as rainfall in region A decreased significantly in the third stage. Moreover, the intense rainfall center shows a northward jump with the discontinuous distribution of rainfall during the transition period from the second stage to the third stage based on the hourly precipitation distribution map (figures omitted). Causes for this northward jump are investigated based on the development and evolution of local convection, TC structure, environmental VWS, and water vapor transportation in this section.

Figure 13 shows the evolution of radar reflectivity during the transition period from 1800 UTC 8 August to 0800 UTC 9 August at 2 h intervals. There were two clearly developing phases of convection. The first was from 1800 UTC 8 August to 0200 UTC 9 August as the TC translated farther inland. The TC inner-core region gradually became drier because of the lack of warm, moist air from the sea. Meanwhile, convection in the inner-core region was restrained, with radar reflectivity weakening further, and the spiral cloud bands dissipated gradually with larger cloud-free areas in the satellite images, which indicates that the TC inner-core was assuming a hollow-core structure. The local severe rainfall in the coastal regions (region A) from central Fujian Province to Wenzhou City, Zhejiang Province decreased dramatically and tended to end under the influence of changes in TC structure. The second phase was from 0400 UTC 9 August to 0800 UTC 9 August, when the outer circulation of the TC in the region from Taizhou City to Ningbo City intensified because of connection to warm, moist air from the sea. At the same time, the west-southwesterly EVWS grew continuously (Figure 11), which facilitated the development of asymmetric convection in the spiral cloud bands at the downshear flank of VWS (Jones, 1995). Furthermore, interaction between the outer circulation of the TC and a mid-latitude trough contributed to the asymmetric distribution of local convective development in the spiral cloud bands of the TC, which cut off the water vapor transportation tunnel to the inner-core area; water vapor distribution showed clear asymmetric features, and the moist area occurred in the northeast quadrant of the TC (region B, Figure 14). In combination with the interaction between the TC outer circulation and local topography (Figure 5c), local convection occurred in the northern part of the outer circulation of the TC in the region from western Anhui Province to the intersection between northwestern Zhejiang Province and southern Jiangsu Province, and to the Siming Mountains in central Zhejiang Province (region B). Correspondingly, the rainfall band presented a northern jump.

Thus, it is evident that the inner-core circulation decayed dramatically because of the reduction of water vapor after TC landfall, especially in the process of translation farther inland. With increasing EVWS, the spiral rainbands in the outer region of TC circulation showed asymmetric development at the downshear flank of EVWS, which blocked water vapor transportation to the inner-core region of the TC. The clouds in the inner-core region dissipated and presented a hollow-core structure. The outer circulation of the TC was maintained and developed because of connection with the southerly warm and moist flow from the sea. With the interaction between the outer circulation of the TC and local topography, the severe rainfall region jumped northward.

3.5 The effect of interaction between TC circulation and the mid-latitude system on the rapid reduction of rainfall in Zhejiang Province in the fourth stage

Figure 2a shows that there were two regions of severe rainfall after landfall of Soudelor in mainland China. One was located in the region from central Fujian Province to central Zhejiang Province, and another was located in central Jiangsu Province. Analysis of Figures 3, 4c and 4d indicates that the intense precipitation in central Jiangsu Province occurred because of the interaction between the outer cir-

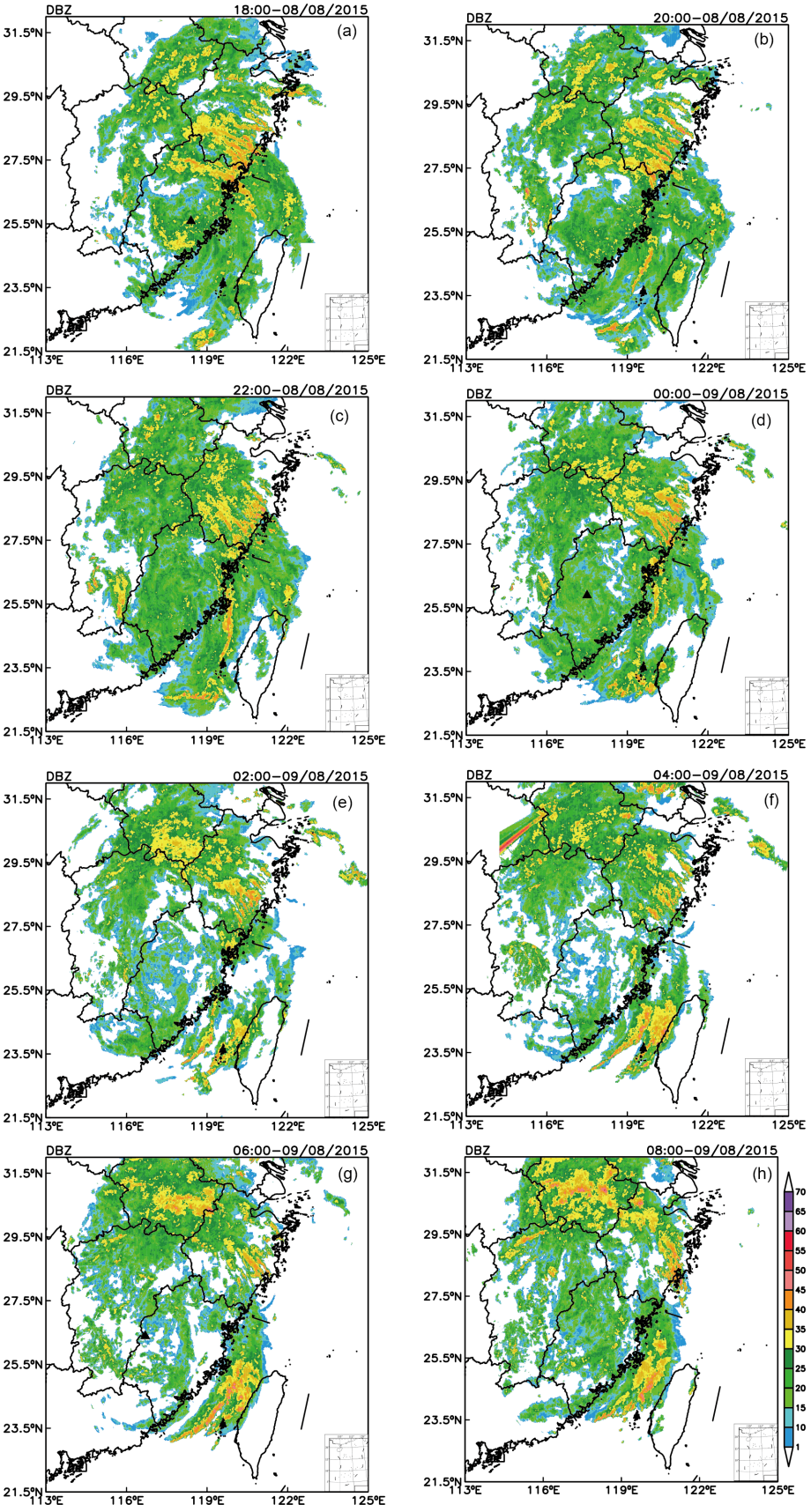

Figure 13 Time evolution of Radar reflectivity (unit: dbz) at 2 h intervals from 1800 8 to 0800 9 August 2015.

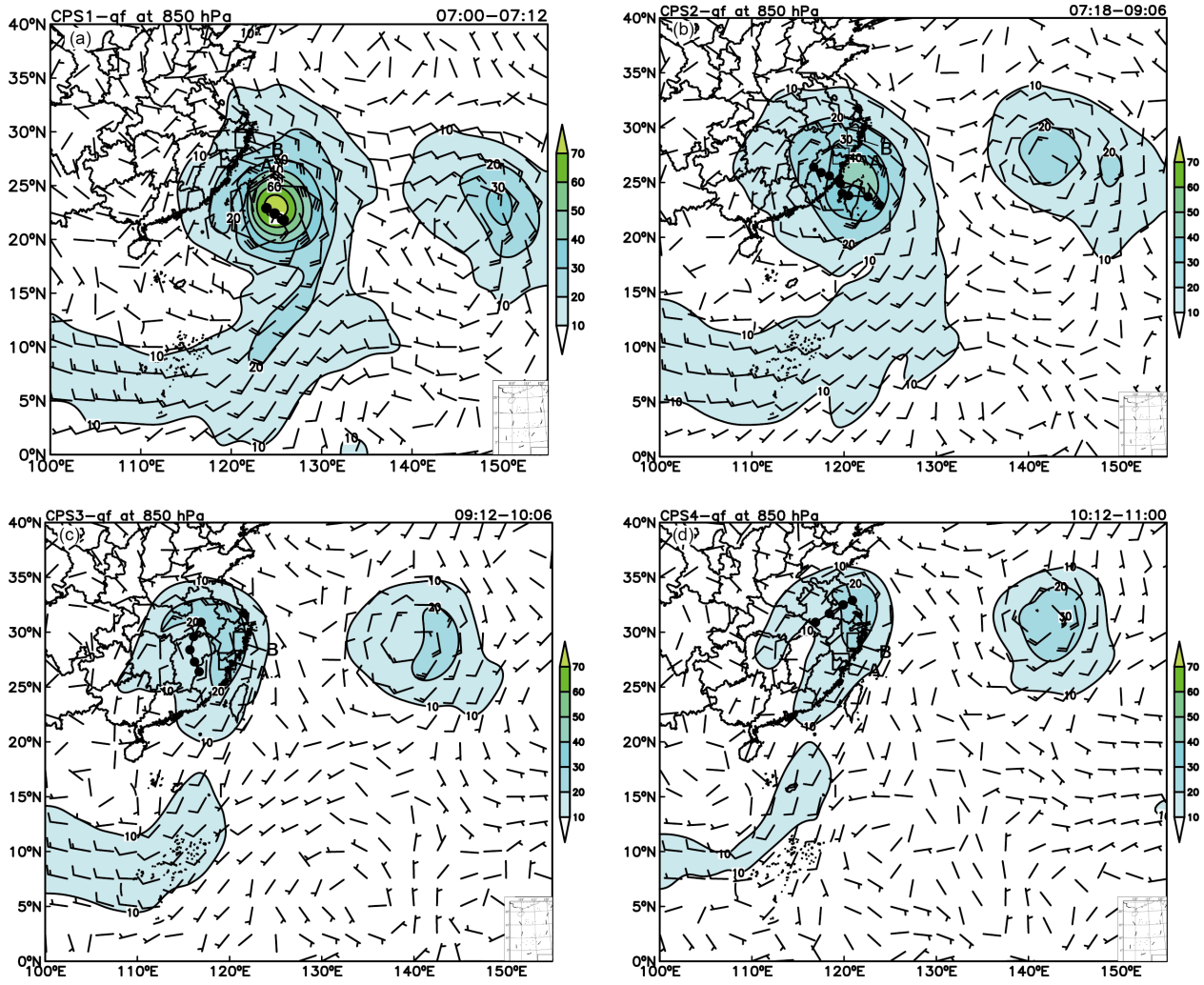

Figure 14 Vapor flux (shading, unit: g cm^{-1} hPa^{-1} s^{-1}) and wind vector (full bar=10 m s^{-1}) at 850 hPa for phases I, II, III, and IV of precipitation of TC Soudelor (1513); rectangles indicate precipitation areas A and B.

culation of the TC and a mid-latitude system during the transition period from the third stage to the fourth stage of rainfall. As the fourth stage of rainfall began, the precipitation in central Jiangsu Province increased rapidly, whereas rainfall in Zhejiang Province decreased rapidly. Extratropical transition (ET) of a TC occurs as TC circulation interacts with mid-latitude weather systems, and the precipitation produced in the process of ET behaves with distinct baroclinic characteristics. The effects of the interaction between TC circulation and mid-latitude weather systems on local severe precipitation can be investigated by calculating the frontogenesis function (FGF) of eq. (3) (Petterssen, 1936; Doswell et al., 1996; Harr et al., 2000; Harr and Elsberry, 2000; Colle, 2003; Gao et al., 2009):

$$F = \frac{\mathrm{d}}{\mathrm{d}t}\left|\nabla_h \theta\right| = \frac{-1}{\left|\nabla_h \theta\right|}\left\{\left[\left(\frac{\partial \theta}{\partial x}\right)^2\left(\frac{\partial u}{\partial x}\right) + \left(\frac{\partial \theta}{\partial y}\right)^2\left(\frac{\partial v}{\partial x}\right)\right] + \left[\frac{\partial \theta}{\partial x}\frac{\partial \theta}{\partial y}\left(\frac{\partial v}{\partial x} + \frac{\partial u}{\partial y}\right)\right]\right\}, \quad (3)$$

where θ represents potential temperature, and u and v indicate the components of the x and y axis in a Cartesian coordinate system, respectively.

Figure 15 shows the distributions of the FGF in different stages of rainfall. In the first and second stages of rainfall, wind velocity and directional shear were induced by the different friction effects from the sea and land surfaces to the land side of the western half of the TC. Differences between sea and land surfaces can causes the lift of TC circulation and the release of weak instability energy within the TC (Houze, 2010, 2012), which increase the gradient of the FGF, intensify the centers of frontogenesis, and eventually lead to asymmetric distribution of precipitation in these two stages of rainfall. There was no apparent frontogenesis in the third

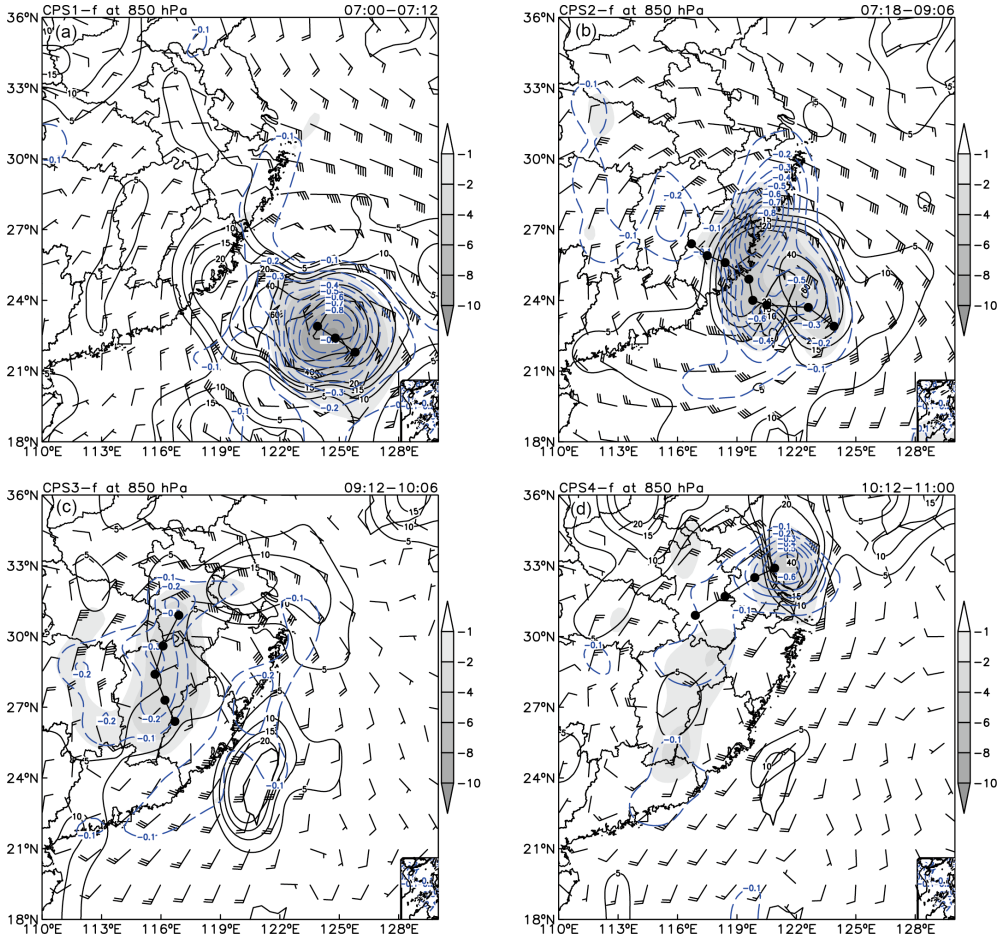

Figure 15 The frontgenesis function (solid line, 10^{-10} K m^{-1} s^{-1}), wind vector field (full bar=10 m s^{-1}), divergence (shaded, 10^{-5} s^{-1}), and vertical velocity (dotted line, hPa s^{-1}) at 850 hPa in rainfall phases I (a), II (b), III (c), and IV (d) of TC Soudelor.

stage of rainfall in Zhejiang Province, which indicates that precipitation in this stage was not instability rainfall induced by the invasion of mid-tropospheric cold air into TC circulation, but resulted from cyclonic circulation caused by the wind velocity and directional shear of strong winds and orographic effects. In the fourth stage, the major rainfall zone shifted northward to central Jiangsu Province with the occurrence of evident overlapping areas of frontogenesis, convergence, and vertical upward motion, which resulted directly from the interaction between the TC outer circulation and the mid-latitude trough. It should be noted that the severe rainfall area does not coincide with large values of the FGF, but with the overlapping region of the FGF, convergence, and vertical upward motion, which demonstrates that the enhancement of local severe rainfall resulted from the development of local convection associated with increased vertical upward motion induced by the combined effects of the release of baroclinic potential energy and the enhancement of local convergence. However, the primary water vapor transportation area shifted from region B northward to central Jiangsu Province in the third stage because of increasing local wind velocity and convergence resulting from the interaction between TC circulation and the mid-latitude weather system (Figure 14d). Moreover, the EVWS was westerly and reached its maximum in the fourth stage (Figure 11b), and the weak convection systems located in the coastal region of Zhejiang province shifted eastward to the sea under the influence of EVWS. Local convection and water vapor transportation in Zhejiang Province decreased rapidly, and rainfall weakened quickly and tended to end (Figures 3 and 4d). Furthermore, the zonal-vertical cross-section of potential temperature (Figure 16) in the previous stages of rainfall shows that there was weak northwesterly intrusion in the western side of TC circulation, which formed a weak frontogenesis area only in the second stage, and resulted in weak local, asymmetric precipitation (Figure 16b). The TC was modulated by southeasterly (Figure 16a) or westerly (Figure 16e, g) winds in the first and third stages of rainfall. In the meridional-vertical cross-section of potential temperature, there was no frontogenesis in the three previous stages of rainfall, but a cold front extending from surface to 500 hPa appeared in the north flank of the TC center in the fourth stage. Northerly wind prevailed in the area south of 36°N, and transported the air mass with high instability and

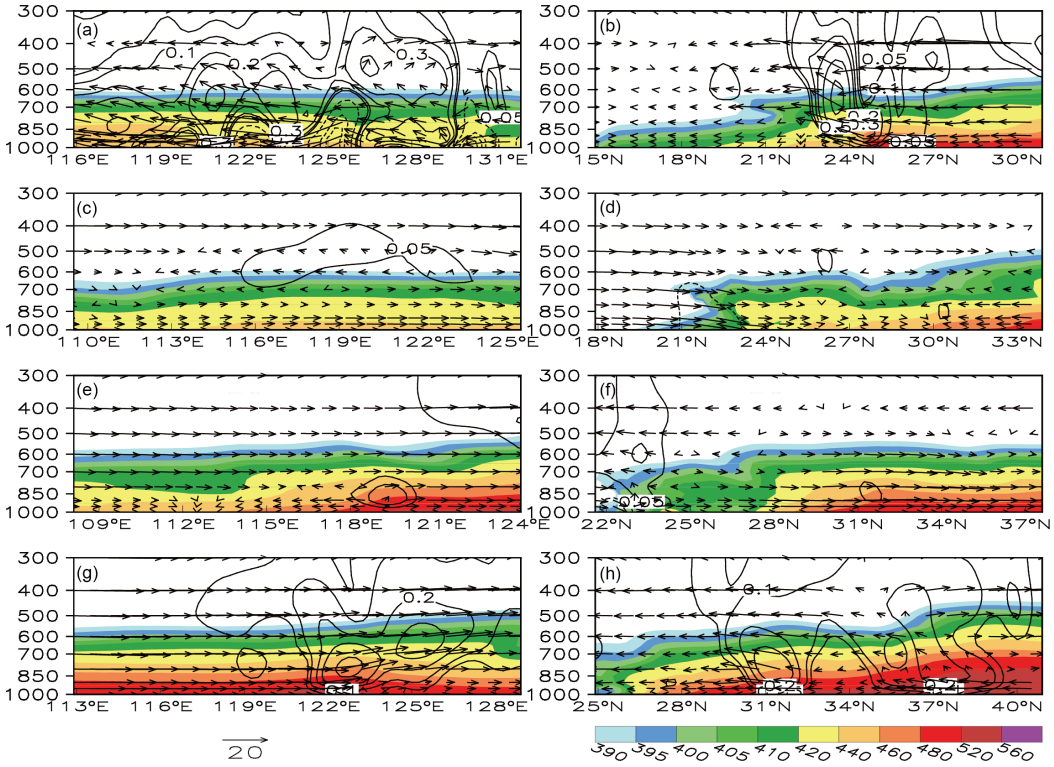

Figure 16 Zonal-vertical ((a), (c), (e), (g)) and meridional-vertical ((b), (d), (f), (h)) cross-sections of equivalent potential temperature (shaded, unit: K), vertical velocity (black solid contours, unit: m s^{-1}) and wind vector field (m s^{-1}) through the TC center in each rainfall phase. Black solid delta denotes the TC center, *Y*-axis represents pressure in units of hPa; abscissa indicates longitude (latitude) in (a), (c), (e), (g) ((b), (d), (f), (h)).

water vapor to around 26°N. The instability in the middle-lower troposphere increased, and a strong upward-motion center formed near 31°N to 32°N, which resulted in the occurrence of local severe rainfall in central Jiangsu Province in the last stage of rainfall.

In summary, the new rainfall center located in central Jiangsu Province, caused by the interaction between TC outer circulation and the mid-latitude weather system as the TC translated northward, made the moist area shift northward and resulted in a dramatic drop in the transportation of water vapor and convection development in Zhejiang Province. Combined with the enhancement of EVWS, the weak convective systems induced by the interaction between the TC remnant vortex and the mountainous topography in the eastern coastal region of Zhejiang Province translated quickly to the sea, which led to the end of rainfall.

3.6 The role of the quasi-circular TC track in the formation of local extreme rainfall

Accumulated precipitation can be estimated using eq. (4):

$$R_a = \bar{r} \times t, \quad (4)$$

where, R_a is the accumulated precipitation in units of mm; $\bar{r}$ represents the mean rainfall rate during the rainfall period, and t is duration of rainfall.

Figure 3 shows the evolution over time of the area-averaged hourly rainfall rate of Soudelor. Compared with the rainfall that resulted from other TCs with disastrous impacts in Zhejiang Province, the hourly rainfall rate caused by Soudelor was not the greatest, but the total accumulated precipitation was maximized. Aside from the sustained extreme rainfall induced by TC circulation in the second stage, the classic track of the TC was closely related to the maximum accumulated precipitation (Figure 2). The TC track of Soudelor presents a quasi-circular trajectory centered around the southeastern coast of Zhejiang province during the period from its landfall on Taiwan to its translation over the sea from central Jiangsu Province. This specific quasi-circular track facilitated the maintenance of a high rainfall rate generated from the outer circulation and principal rainbands of Soudelor for a relatively long period of time in the rainfall region of Zhejiang Province. A high rainfall rate sustained for a long period of time can result in local extreme precipitation according to eq. (4).

Figure 17 shows the composite distribution of geopotential height and wind vectors at 500 hPa for each stage of rainfall, and can be utilized to investigate the shape change of the Western Pacific Subtropical High (WPSH) and the effect of environmental steering flow on TC track. In the first stage, the WPSH formed a high dam in the north of Zhejiang Province with the western ridge point located at central Anhui Province, and the TC was steered westward by east-

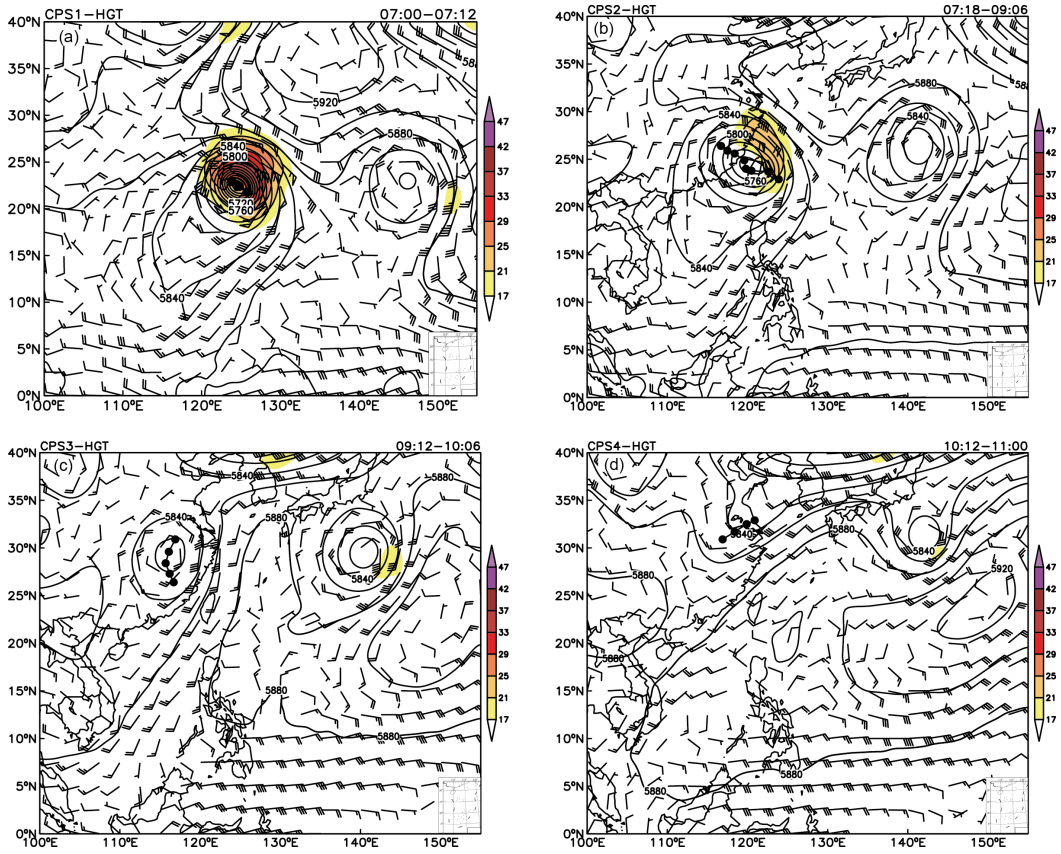

Figure 17 Composite of geopotential height (with interval of 2 gpm) and wind vector field (full bar=10 m s^{-1}) at 500 hPa (shading indicates wind velocity, unit: m s^{-1}).

erly winds in the southern flank of the WPSH. In the second stage, the WPSH retreated northeastward under the influence of the northward-translating Typhoon Molave (1514), which resulted in the breakdown of the high dam. The TC translated west-northwestward, modulated by the east-southeast steering flow in the southwest of the WPSH. The WPSH broke again because of its location between two TCs, and the orientation of the WPSH shifted from latitudinal to longitudinal; thus, the TC turned northward as it entered Jiangxi Province, steered by the southerly wind in the southwest flank of the WPSH in the third stage. In the last stage of rainfall, the WPSH fell southward, extended westward, and merged with the remnant high over mainland China. Soudelor turned northeastward, steered by the southwesterly flow in the northwest of the WPSH. The intensity of the steering flow remained around 12 m s^{-1} during the whole rainfall process of the TC. The translation speed of the TC increased rapidly during the later rainfall stages because of the continuous decrease of TC intensity after landfall under the influence of the same intensity of steering flow. It follows that the change of steering flow induced by the shape and location change of the WPSH was the key factor determining the quasi-circular track of Soudelor during the rainfall period in Zhejiang Province. The quasi-constant speed of steering flow caused the distinct difference of the TC's translation speed in different stages of rainfall as the TC continuously decayed, which led to different sustained durations of rainfall in each stage. In addition, the abnormal track of the TC in the second stage, first translating southward over Taiwan and then northward in the Taiwan straits, was one of the most important factors that resulted in severe precipitation in this stage, which was closely related to orographic effects (Xie and Zhang, 2012). Furthermore, the distance between the severe rainfall regions, including regions A and B in Zhejiang Province, and the center of the TC remained between 300 and 600 km after the TC made landfall in Taiwan, until it translated over the sea from Jiangsu Province, and the track of the TC presented a generally quasi-circular, clockwise trajectory surrounding point C, which was the mid-point between regions A and B.

The quasi-circular track of the TC surrounding the rainfall regions induced by the change of the WPSH caused the rainfall regions to be covered by the convective outer rainbands of the TC during the period of severe local precipitation, from 1200 UTC 7 August to 0600 UTC 10 August 2015, which resulted in large amounts of accumulated rainfall. In addition, an important reasons for the intense precipitation in region A in the second stage was the long-term (around 42 h) maintenance of the intense rainbands. There are two main reasons for the long-lasting maintenance of

intense rainbands. One was the abnormal track of the TC, first moving southwestward after crossing Taiwan and then turning north-northwestward across the Taiwan Straits, and finally making landfall in central Fujian Province with northwestward movement. The track of the TC led to local weak convection in region A because of the interaction between the outer TC circulation and the local topography of Yandang Mountain early in the second stage of rainfall (Figure 18a), and the corresponding rainfall accumulation was small (Figure 10). Convection intensified significantly, and the rainbands shifted from outer TC circulation to the principal rainband of the outer section of the TC in region A (Figure 18b and c) and reached maxima prior to the second landfall, while the principal rainband affected region A (Figure 18d). Afterward, the intensity of Soudelor decayed gradually as it translated westward, and region A was modulated by the principal rainband of the TC. This track of the TC was favorable for the occurrence of sustained rainfall induced by the intense convection of rainbands in the right flank of the TC over a long period of time in region A. Secondly, the VWS was relatively low as the TC translated westward after making landfall. The structure of the TC did not tilt, and the intensity decreased slowly, with the TC remaining a typhoon to severe tropical storm, and the change of environmental steering flow was slight. All of these factors slowed down the translation speed of the TC and increased the length of time for the maintenance of intense rainband of the TC in region A, and thus resulted in maximal accumulated precipitation in the second stage. Studies by Chen et al. (2010) and Chen and Xu (2017) have shown that the significant characteristics of TCs resulting in extreme precipitation are that the TC translates slowly, connects with an intense water vapor tunnel, and maintains quasi-constant intensity that decays little. In the above analysis, the characteristics of the intensity and track of Soudelor in the second stage in Zhejiang Province were consistent with the characteristics necessary for the formation of extreme torrential rainfall according to Chen et al. (2010) and Chen and Xu (2017) in the second stage.

The above analyses show that several characteristics were responsible for the formation of local extreme precipitation in Zhejiang Province. The first was that the convective system decayed slowly in a relatively stable large-scale environment where vertical upward flow continuously transported water vapor from the sea to above the convection condensation level (CCL), which formed severe local rainfall. Secondly, the interaction between TC circulation and the mountainous topography maintained and enhanced the convective systems, and led to sustained severe local rainfall combined with warm moisture transportation from the sea. Thirdly, the quasi-circular track of the TC centered around the local severe rainfall area, which resulted from the change of the WPSH, caused the severe rainfall area within 300–600 km from the TC center to remain under the influence of the principal rainbands of the TC during the entire period, which resulted in maximal accumulation of precipitation. Lastly, baroclinic rainfall induced by the interaction of TC circulation and the mid-latitude weather system made the rainbands shift northward, which directly led to the end of rainfall in Zhejiang Province.

4. Conclusions

Typhoons are among the most disastrous weather systems in East China. Typhoon precipitation and its secondary disasters are the most severe of all meteorological disasters. Super Typhoon Soudelor (2015) produced local severe rainfall in the central and southern coastal regions of Zhejiang Province, and caused some of the most intense precipitation caused by any TC on record in Zhejiang Province. Flash flooding and mudslides induced by the local severe rainfall of Soudelor resulted in 14 fatalities and over 8 billion CNY in direct economic damage. Many characteristics of Soudelor's rainfall differed from other TCs affecting Zhejiang Province. To elucidate the reasons for the extreme torrential rainfall caused by Typhoon Soudelor, the major impacting factors and dynamics associated with Soudelor (2015) that led to local severe precipitation in East China have been investigated in detail, especially in Zhejiang Province, based on high-resolution mesoscale surface observations, radar reflectivity, FY2E satellite infrared nephograms, and NCEP GFS grid data with 0.25°×0.25° horizontal resolution. The main results show that:

(1) The convection that developed in most previous TCs was strong and covered large areas with intense hourly rainfall rates, but the intervals of time over which local severe rainfall was maintained were relatively short. Comparatively, the vertical upward motion that occurred in the circulation of Soudelor developed mainly in the lower troposphere, and the corresponding intensity of convection was moderate, with relatively low hourly rainfall rates, but the time over which local severe rainfall persisted was longer (around 42 h), which led to maximum accumulation. The intense rainfall process associated with Soudelor presented clear stage characteristics. In the first stage, the TC was located over the ocean east of Taiwan, about 800 km from the rainfall areas in Zhejiang Province. Northeasterly winds prevailed in the rainfall areas, and the rainfall was small, belonging to a category of rainfall distant from the TC that resulted from interaction between outer TC circulation and the coastal mountainous topography in Zhejiang Province in the first stage. The rainfall rate in Zhejiang Province in the second stage was largest, and the accumulated precipitation was maximized because of the principal rainband of the TC. The maintenance of the water vapor tunnel as the TC decayed significantly, combined with the vertical upward mo-

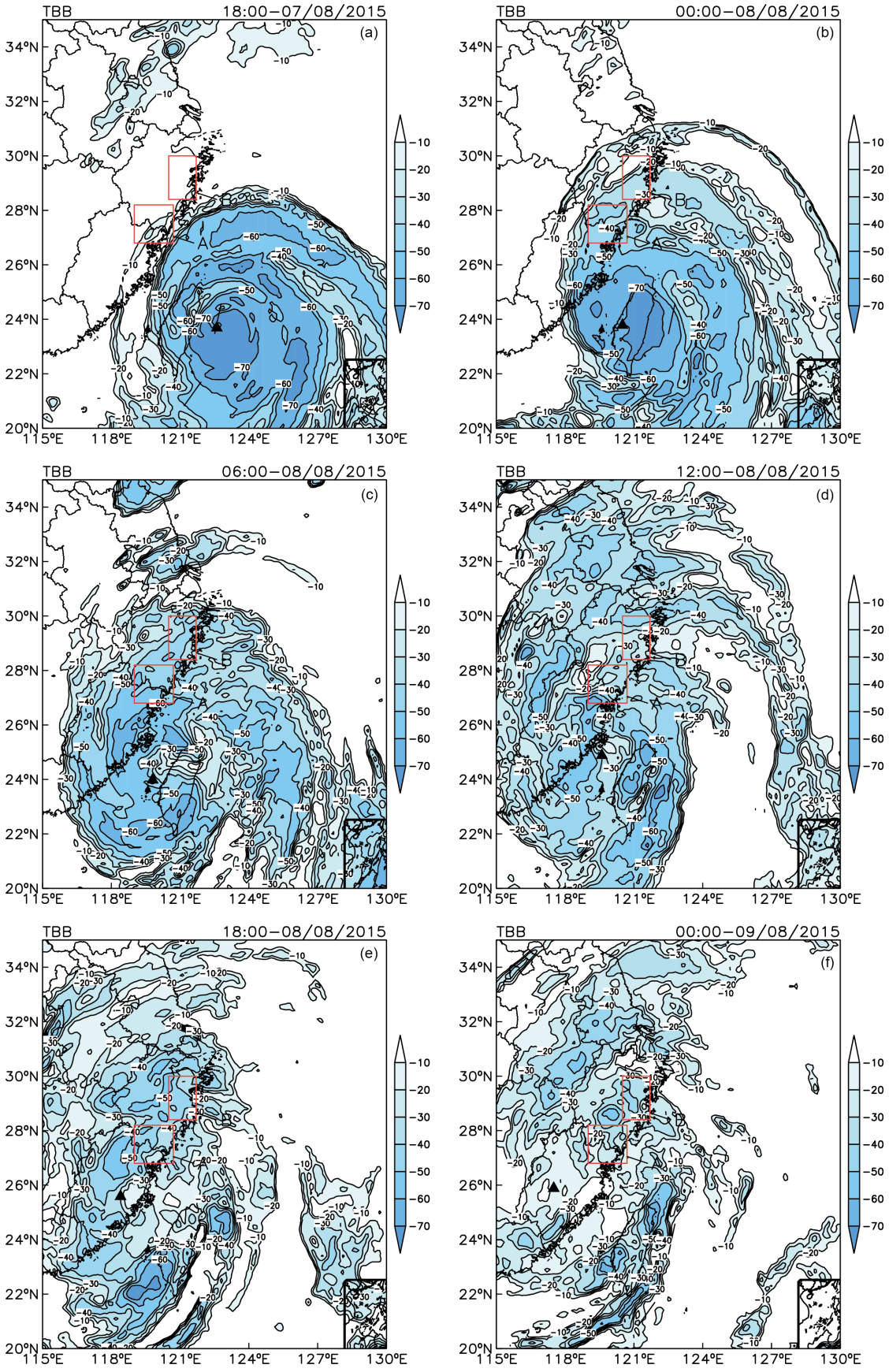

Figure 18 Black body temperature equivalent (TBB, unit: °C) evolution during the second rainfall stage of typhoon Soudelor (black solid triangle denotes the typhoon center).

tion induced by local wind shear and the lifting that resulted from local topography, led to local severe precipitation in the third stage. The interaction between the circulation of the TC and a mid-latitude weather system in the fourth stage shifted water vapor from the sea and the TC rainbands northward, and led to the end of rainfall in Zhejiang Province.

(2) In the classic model of how VWS influences TC rainfall distribution, extreme rainfall is located in the downshear left flank (Jones, 1995). The results in this paper show that the TVWS and EVWS were easterly (southerly) in the severe rainfall period; thus, in the second stage and early in the third stage of rainfall, and the extreme rainfall area was located in the downshear right flank, which indicates that the effect of topography on the asymmetric distribution of TC rainfall was far greater than that induced by VWS in the context of the interaction between TC circulation and local topography. Quantitative calculation of the orographic rainfall rate shows that the contribution to total precipitation from orographic effects may exceed 50%.

(3) In the later period of rainfall, the direction of VWS shifted from southerly to westerly, and the intensity of the VWS increased gradually, which made the spiral rainbands of the TC extend northward, and combined with interactions between the northern flank circulation of the TC and mid-latitude weather system. As a result, the asymmetric structure of TC circulation developed further. A latitudinal distribution of intense wind bands formed in the northern flank of the severe local rainfall area, or the northeast quadrant of TC circulation in Zhejiang Province. With the combined effects of the cyclonic shear of intense wind velocity bands and forcing from local topography, the spiral rainband of the TC extended north-northeastward, which cut off water vapor transportation to the inner-core area of the TC. This phenomenon presented as a northward jump of the severe local rainfall band.

(4) The quasi-circular clockwise track of the TC surrounding the severe local rainfall area in Zhejiang Province induced by the shape and location change of the WPSH prolonged the sustained time of local severe rainfall in Zhejiang Province to around 42 h, which was the dominant factor to cause the extreme accumulated precipitation in Zhejiang Province. However, in contrast to other TCs affecting Zhejiang Province, the interaction between the outer circulation of Soudelor and the mid-latitude weather system occurred in a later stage of rainfall in central Jiangsu Province, and thus had no impact on local rainfall in Zhejiang Province. The characteristics of the relatively low rainfall rate, primary vertical upward motion in the lower troposphere, and the maximal radar reflectivity appearing below 5 km further indicate that the primary reason for the local extreme precipitation of this TC was not the intense convective system, but the combined effects of multiple factors, including the moderately intense TC circulation in the lower troposphere and its interaction with local topography, as well as the rainfall convective system persisting for a long period of time.

Thus, the formation of severe local rainfall that resulted from Typhoon Soudelor in Zhejiang Province was a complex process with multiple factors interacting. This study explored the possible mechanisms responsible for the extreme rainfall in Zhejiang Province that resulted from Typhoon Soudelor based on different elements and their non-linear interactions. The results reported in this paper are expected to further promote understanding, prediction, and prevention of disasters resulting from TC precipitation, especially warnings for flood disasters, including torrential rainfall, mountain flooding, mudslides, and related disasters.

Acknowledgements *This work was supported by the Huadong Regional Meteorological Science and Technology Innovation Fund Collaborative Project (Grant No. QYHZ201404), the Development of Social Welfare Project of Zhejiang Province (Grant No. 2013C33037), the Science Foundation of Zhejiang Province (Grant No. LY18D050001), and United States Office of Naval Research Project (Grant No. N000140910526), the Development of Social Welfare Key Project of Zhejiang Province (Grant No. 2017C03035).*

References

Chen L S. 2007. Research and forecast on rainstorm of landfalling tropical cyclone (in Chinese). National Seminar On Tropical Cyclone Science (NWTC-XIV). 3–7

Chen L S, Ding Y H. 1979. An Introduction to Western North Pacific Typhoon (in Chinese). Beijing: Science Press. 440–442

Chen L S, Li Y. 2004. An overview on the study of the tropical cyclone rainfall. In: Proceedings of International Conference on Storms, Australian Meteorological and Oceanographic Society. Brisbane. 112–113

Chen L S, Li Y, Cheng Z Q. 2010. An overview of research and forecasting on rainfall associated with landfalling tropical cyclones. Adv Atmos Sci, 27: 967–976

Chen L S, Luo Z X, Li Y. 2004. Research advances on tropical cyclone landfall process (in Chinese). Acta Meteorol Sin, 62: 541–549

Chen L S, Meng Z Y. 2001. An overview on tropical cyclone research progress in China during the past ten years (in Chinese). Chin J Atmos Sci, 25: 420–432

Chen L S, Xu X D, Luo Z X, Wang J Z. 2002. Introduction to Tropical Cyclone Dynamics (in Chinese). Beijing: Science Press. 100–108

Chen L S, Xu Y L. 2017. Review of typhoon very heavy rainfall in China (in Chinese). Meteorol Environ Sci, 40: 3–10

Chen S S, Knaff J A, Marks Jr. F D. 2006. Effects of vertical wind shear and storm motion on tropical cyclone rainfall asymmetries deduced from TRMM. Mon Weather Rev, 134: 3190–3208

Chih C H, Chou K H, Chiao S. 2015. Topography and tropical cyclone structure influence on eyewall evolution in Typhoon Sinlaku (2008). Terr Atmos Ocean Sci, 26: 571–586

Colle B A. 2003. Numerical simulation of the extratropical transition of Floyd (1999): Structural evolution and responsible mechanisms for the heavy rainfall over the northeast United States. Mon Weather Rev, 131: 2905–2926

Cong C H, Chen L S, Lei X T. 2011. An overview on the study of tropical cyclone remote rainfall (in Chinese). J Trop Meteorol, 27: 264-270

Corbosiero K L, Molinari J. 2002. The Effects of vertical wind shear on the distribution of convection in tropical cyclones. Mon Weather Rev, 130: 2110–2123

Corbosiero K L, Molinari J, Aiyyer A R, Black M L. 2006. The structure and evolution of hurricane elena (1985). Part II: Convective asymmetries and evidence for vortex rossby waves. Mon Weather Rev, 134:

3073–3091
Dong M Y, Chen L S, Zheng P Q, Pan J S. 2009. Research progress on abrupt intensification of heavy rainfall and super heavy rainfall associated with landfalling tropical cyclones (in Chinese). J Trop Meteorol, 25: 495–502
Doswell Iii C A, Brooks H E, Maddox R A. 1996. Flash flood forecasting: An ingredients-based methodology. Weather Forecast, 11: 560–581
Duan W L, He B, Nover D, Fan J, Yang G, Chen W, Meng H F, Liu C M. 2016. Floods and associated socioeconomic damages in China over the last century. Nat Hazards, 82: 401–413
Emanuel K A. 2005. Increasing destructiveness of tropical cyclones over the past 30 years. Nature, 436: 686–688
Fan Q, Liang B Q. 2000. A fuzzy mathematics evaluation of disastrous economic losses caused by tropical cyclones (in Chinese). Sci Meteorol Sin, 20: 360–366
Frank W M, Ritchie E A. 1999. Effects of environmental flow upon tropical cyclone structure. Mon Weather Rev, 127: 2044–2061
Galarneau Jr T J, Bosart L F, Schumacher R S. 2010. Predecessor rain events ahead of tropical cyclones. Mon Weather Rev, 138: 3272–3297
Gao S Z, Meng Z Y, Zhang F Q, Bosart L F. 2009. Observational analysis of heavy rainfall mechanisms associated with severe tropical storm Bilis (2006) after its landfall. Mon Weather Rev, 137: 1881–1897
Hall J D, Xue M, Ran L, Leslie L M. 2013. High-resolution modeling of typhoon Morakot (2009): Vortex Rossby Waves and their role in extreme precipitation over Taiwan. J Atmos Sci, 70: 163–186
Harr P A, Elsberry R L. 2000. Extratropical transition of tropical cyclones over the western North Pacific. Part I: Evolution of structural characteristics during the transition process. Mon Wea Rev, 128: 2613–2633
Harr P A, Elsberry R L, Hogan T F. 2000. Extratropical transition of tropical cyclones over the Western North Pacific. Part II: The impact of midlatitude circulation characteristics. Mon Weather Rev, 128: 2634–2653
Houze Jr R A. 2010. Clouds in tropical cyclones. Mon Weather Rev, 138: 293–344
Houze Jr R A. 2012. Orographic effects on precipitating clouds. Rev Geophys, 50: RG1001
Huang X Q, Teng D G, Lu W. 2014. A preliminary study on the relationship between the distant precipitation and the wave characteristics of typhoon Krosa in Zhejiang Province (in Chinese). Trans Atmos Sci, 37: 57–64
Jiang S C. 1983. A synoptic model of the hardrain storm in westerly belt affected by the far distant typhoon (in Chinese). Acta Meteorol Sin, 41: 147–158
Jones S C. 1995. The evolution of vortices in vertical shear. I: Initially barotropic vortices. Q J R Meteorol Soc, 121: 821–851
Li J N, Wang A Y, Yang Z L, Li G L, He X J, Peng T Y, Gu Z M. 2003. Advancement in the study of typhoon rainstorm (in Chinese). J Trop Meteorol, 19: 152–159
Li Y, Chen L S, Xu X D. 2005. Numerical experiments of the impact of moisture transportation on sustaining of landfalling tropical cyclone and precipitation (in Chinese). Chin J Atmos Sci, 29: 91–98
Li Y, Wang J Z, Chen L S, Yang Y Q. 2007. Study on wavy distribution of rainfall associated with typhoon Matsa (2005). Chin Sci Bull, 52: 972–983
Li Y, Cheung K K, Chan C L. 2015. Modelling the effects of land-sea contrast on tropical cyclone precipitation under environmental vertical wind shear. Q J R Meteorol Soc, 141: 396–412
Lin Y L, Chiao S, Wang T A, Kaplan M L, Weglarz R P. 2001. Some common ingredients of heavy orographic rain-fall. Weather Forecast, 16: 633–660
Luo Z X. 1994. Effect of energy dispersion on structure and motion of tropical cyclone (in Chinese). Acta Meteorol Sin, 52: 149–156
Luo Z X. 2005. Typhoon self-organization in multi-scale coexisting system (in Chinese). Acta Meteorol Sin, 63: 672–682
Luo Z X, Ma G L, Ping F. 2010. Investigation of fine and complex vortex circulation structures. Sci China Earth Sci, 53: 1552–1558
Meng Z Y, Zhang Y J. 2012. On the squall lines preceding landfalling tropical cyclone in China. Mon Weather Rev, 140: 445–470
Moore L J, McNamara D E, Murray A B, Brenner O. 2013. Observed changes in hurricane-driven waves explain the dynamics of modern cuspate shorelines. Geophys Res Lett, 40: 5867–5871
Munsell E B, Zhang F Q. 2014. Prediction and uncertainty of Hurricane Sandy (2012) explored through a real-time cloud-permitting ensemble analysis and forecast system assimilating airborne Doppler radar observations. J Adv Model Earth Syst, 6: 38–58
Nasrollahi N, Agha K A, Li J L, Gao X G, Hsu K L, Sorooshian S. 2002. Assessing the impacts of different WRF Precipitation physics in hurricane simulations. Weather Forecast, 27: 1003–1016
National Hurricane Center (NHC). The Saffir-Simpson Hurricane wind scale (experimental). http://www.nhc.noaa.gov/aboutsshs.html, 2009
Petterssen S. 1936. Contribution to the theory of frontogenesis. Geofys Publ, 11: 1–27
Qian Y Z, He C F, Yang Y Q, Wang J Z. 2001. An assessment of damage index for tropical cyclone (in Chinese). Meteorol Mon, 27: 14–27
Rogers R, Frank M, Timothy M. 2009. Tropical Cyclone Rainfall. Encyclopedia of Hydrological Sciences. Chichester: John Wiley & Sons, Ltd. 1–22
Shi P J. 2016. Natural Disasters in China. Beijing: Springy and Beijing Normal University Press. 103
Smith R B. 1979. The influence of mountains on the atmosphere. Adv Geophys, 21: 87–230
Tao D D, Zhang F Q. 2014. Effect of environmental shear, sea-surface temperature, and ambient moisture on the formation and predictability of tropical cyclones: An ensemble-mean perspective. J Adv Model Earth Syst, 6: 384–404
Tao D, Zhang F Q. 2015. Effects of vertical wind shear on the predictability of tropical cyclones: Practical versus intrinsic limit. J Adv Model Earth Syst, 7: 1534–1553
Tao S Y. 1980. Heavy rainfall in China (in Chinese). Beijing: Chinese Science Press. 225
Tao S Y, Ding Y H, Zhou X P. 1979. The present status of the research on heavy rainfall and convection weather (in Chinese). Chin J Atmos Sci, 3: 227–238
Teng D G, Luo Z X, Li C H, Yu H, Dai K. 2009. Typhoon vortex self-organization in a baroclinic environment. Acta Meteorol Sin, 23: 539–549
Wang Y P, Cui X P, Ran L K,Yu H. 2015. Cloud microphysical characteristics of different precipitation types in Bilis (0604) torrential rainfall events (in Chinese). Chin J Atmos Sci, 39: 548−558
Wang Z M. 2013. Handbook of Weather Forecasting in Zhejiang Province (in Chinese). Beijing: Meteorological Press. 75–99
Wong M L M, Chan J C L. 2004. Tropical cyclone intensity in vertical wind shear. J Atmos Sci, 61: 1859–1876
Xie B G, Zhang F Q. 2012. Impacts of typhoon track and island topography on the heavy rainfalls in Taiwan associated with Morakot (2009). Mon Weather Rev, 140: 3379–3394
Xu W, Zhuo L, Zheng J, Ge Y, Gu Z, Tian Y. 2016. Assessment of the casualty risk of multiple meteorological hazards in China. Int J Environ Res Public Health, 13: 222
Zhang F Q, Tao D D. 2013. Effects of vertical wind shear on the predictability of tropical cyclones. J Atmos Sci, 70: 975–983
Zhang Q H, Wei Q, Chen L S. 2010. Impact of landfalling tropical cyclones in mainland China. Sci China Earth Sci, 53: 1559–1564
Zhu Q H, Zhang S Y, Gu Q M, Wu Z H. 1992. Prediction of Disaster Weather in Zhejiang Province (in Chinese). Beijing: China Meteorological Press. 42–48

(Responsibility editor: Dehai LUO)